Acta Biochimica Polonica

Vol. 50 No. 2/2003

337–365

QUARTERLY

Review

The structure of the Ca^{2+}-ATPase of sarcoplasmic reticulum✪

Anthony N. Martonosi[1] and Slawomir Pikula[2]✉

[1]*State University of New York, Upstate Medical University, College of Graduate Studies, Syracuse, New York, U.S.A.;* [2]*M. Nencki Institute of Experimental Biology, Polish Academy of Sciences, Warszawa, Poland*

Received: 30 May, 2003; accepted: 02 June, 2003

Key words: calcium homeostasis, sarcoplasmic reticulum, calcium pump, calcium transport, excitation-contraction coupling, skeletal and cardiac muscles

In this article the morphology of sarcoplasmic reticulum, classification of Ca^{2+}-ATPase (SERCA) isoenzymes presented in this membrane system, as well as their topology will be reviewed. The focus is on the structure and interactions of Ca^{2+}-ATPase determined by electron and X-ray crystallography, lamellar X-ray and neutron diffraction analysis of the profile structure of Ca^{2+}-ATPase in sarcoplasmic reticulum multilayers. In addition, targeting of the Ca^{2+}-ATPase to the sarcoplasmic reticulum is discussed.

The classical studies of Heilbrunn and Wierczinsky (1947), Ebashi (1961; 1962), Hasselbach (1961; 1963) and Weber (1959; 1964) on the Ca^{2+} regulation of muscle contraction by the sarcoplasmic reticulum (SR) set the stage for the exploration of the unique

✪This work was supported in part by grant No. 3 P04A 007 22 from the State Committee for Scientific Research (KBN, Poland).

✉Corresponding author: Slawomir Pikula, Department of Cellular Biochemistry, M. Nencki Institute of Experimental Biology, L. Pasteura 3, 02-093 Warszawa, Poland; tel.: (48 22) 659 8571 (ext. 347); fax: (48 22) 822 5342; e-mail: slawek@nencki.gov.pl

Abbreviations: AMPPCP, 5′-[beta,gamma-methylene]triphosphate; AMPPNP, adenosine 5′-(beta,gamma-imino)triphosphate; BiP, immunoglobulin binding protein; caged ATP, P^3-1(2-nitro)phenylethyladenosine-5′-triphosphate; DHPR, dihydropyridine receptor; ER, endoplasmic reticulum; FITC, fluorescein-5′-isothiocyanate; PLN, phospholamban; PMCA, plasma membrane Ca^{2+}-ATPase; RyR, ryanodine receptor; SERCA, sarco(endo)plasmic reticulum Ca^{2+}-ATPase; SR, sarcoplasmic reticulum; TG, thapsigargin; TNP-AMP, 2′,3′-*O*-(2,4,6-trinitrophenyl)AMP; 8-azido-TNP-ATP, 8-azido-2′,3′-*O*-(2,4,6-trinitrophenyl)ATP; V, vanadate; T-tubules, transverse tubules.

role of calcium in the regulation of a wide range of metabolic processes and for the elucidation of mechanisms by which cytoplasmic and intraorganellar Ca^{2+} concentrations are controlled in living cells.

THE MORPHOLOGY OF SARCOPLASMIC RETICULUM

The SR of skeletal muscle consists of two morphologically and functionally distinct regions: the junctional SR and the free SR (for review see Peachey & Franzini-Armstrong, 1983). The junctional SR membrane contains the ryanodine receptor (RyR) Ca^{2+} channel with feetlike projections on its cytoplasmic surface that interact with the dihydropyridine receptor (DHPR) particles contained in the junctional region of the T-tubules, forming the T-SR (triad or dyad) junction. The T-SR junction is involved in the transmission of the excitatory stimulus from the surface membrane to the SR, causing Ca^{2+} release from the sarcoplasmic reticulum (Martonosi & Pikula, 2003). The free SR contains the Ca^{2+} transport ATPase as its principal membrane component. It is usually divided into the lateral sacs (cisternae), and the longitudinal tubules, which differ in protein composition. The lateral sacs contain electron-dense material in their lumen, which is attributed to the lumenal Ca^{2+}-binding proteins of SR (calsequestrin, calreticulin, high affinity Ca^{2+}-binding proteins, etc.) that may serve as storage sites for the accumulated Ca^{2+}. The slender longitudinal tubules connect the lateral sacs through the center of the sarcomere and across the Z line; they contain little or no calsequestrin.

Differential and sucrose gradient centrifugation permits the separation of the various membrane elements into vesicular fractions enriched in T-tubules, lateral sacs, and longitudinal tubules, which differ in Ca^{2+} transport activity and protein composition (Caswell *et al.*, 1988; Chu *et al.*, 1988; Costello *et al.*, 1988; Mitchell *et al.*, 1988). Among the SERCA Ca^{2+}-ATPase isoenzymes, the SERCA1 and SERCA2a Ca^{2+} transport ATPase isoforms are evenly distributed throughout the free SR and most of the lateral sac, but are apparently excluded from the junctional SR. The SERCA2b isoform may be preferentially localized near the T-SR junction. Detailed classification of SERCA isoforms is described in the next paragraph.

CLASSIFICATION OF Ca^{2+}-ATPase ISOENZYMES

The determination of the amino-acid sequences of the sarcoplasmic reticulum Ca^{2+}-ATPase (MacLennan *et al.*, 1985), and of the closely related Na^{+},K^{+}-ATPase (Kawakami *et al.*, 1985; Shull *et al.*, 1985) has opened a new era in the analysis of ion transport mechanisms. Since 1985 several large families of structurally related ion transport enzymes were discovered that are the products of different genes. Within each family several isoenzymes may be produced from a single gene product by alternative splicing. Our discussion will concentrate on the Ca^{2+} transport ATPases that occur in the SR of muscle cells of diverse fiber types and in the endoplasmic reticulum (ER) of nonmuscle cells.

The sarco/endoplasmic reticulum Ca^{2+}-ATPases of mammalian tissues can be divided structurally into 3 main groups (SERCA1–3) representing the products of different genes.

The SERCA1 gene (ATP2A1) produces two isoforms of the Ca^{2+}-ATPase, that are derived by alternative splicing of the primary gene product (MacLennan *et al.*, 1985; Brandl *et al.*, 1986). SERCA1a denotes the Ca^{2+}-ATPase of adult fast-twitch skeletal muscle with glycine at its C-terminus in the rabbit (Brandl *et al.*, 1987; Korczak *et al.*, 1988), and alanine in the chicken (Ohnoki & Martonosi, 1980; Karin *et al.*, 1989). The C terminus of the lobster enzyme is apparently blocked (Ohnoki & Martonosi, 1980). SERCA1b is the alterna-

tively spliced neonatal form of SERCA1, in which the glycine at the C-terminus is replaced by the alternative sequence -Asp-Pro-Glu-Asp-Glu-Arg-Arg-Lys (Brandl *et al.*, 1986; 1987). The gene encoding SERCA1 is on human chromosome 16 (MacLennan *et al.*, 1987). A selective defect in its expression is the cause of some forms of Brody's disease (MacLennan, 2000).

The SERCA2 gene (ATP2A2) also produces at least two isoforms that are tissue specific. SERCA2a is the principal form of the Ca^{2+}-ATPase in adult slow-twitch skeletal and cardiac muscles and in neonatal skeletal muscles (Barndl *et al.*, 1986; MacLennan *et al.*, 1987; Lytton *et al.*, 1988; 1992; Wu *et al.*, 1995; Verboomen *et al.*, 1995). It is also expressed at much lower levels in nonmuscle cells (Wu *et al.*, 1995). Its C-terminus is Pro-Ala-Ile-Leu-Glu. SERCA2b is an alternatively spliced product of the same gene (Gunteski-Humblin *et al.*, 1988; Lytton *et al.*, 1989). It is located primarily in nonmuscle tissues and in smooth muscles, where it serves as the major intracellular Ca^{2+} pump. SERCA2b is characterized by a long C-terminal extension of 50 amino acid residues ending in Trp-Ser (Gunteski-Humblin *et al.*, 1988; Lytton *et al.*, 1988; 1989). The gene for both forms of SERCA2 is located on human chromosome 12 (MacLennan *et al.*, 1987). Its expression is not affected in Brody's disease, suggesting that the two major forms of SR Ca^{2+}-ATPases are independently regulated.

SERCA3 is encoded by the ATP2A3 gene (Dode *et al.*, 1996). It is broadly distributed in skeletal muscle, heart, uterus, and in a variety of nonmuscle cells (Burk *et al.*, 1989; Wuytack *et al.*, 1995; Dode *et al.*, 1996; Kovacs *et al.*, 2001). The mRNA levels are particularly high in intestine, lung and spleen, while it is very low in liver, testes, kidney and pancreas. In the muscle tissue SERCA3 may be confined primarily to nonmuscle cells (endothelial cells, etc.). The C-terminus of SERCA3 is Asp-Gly-Lys-Lys-Asp-Leu-Lys; it may serve as a sorting signal for retention of the enzyme in the endoplasmic reticulum (Burk *et al.*, 1989).

Sequences of SERCA type Ca^{2+}-ATPases were also obtained from *Plasmodium yoelii* (Murakami *et al.*, 1990), *Artemia* (Palmero *et al.*, 1989), and *Drosophila* (Magyar *et al.*, 1995). These enzymes are similar in size to SERCA type Ca^{2+}-ATPases from mammalian muscles, but based on their N- and C-terminal sequences they represent a distinct group. In spite of the wide phylogenetic variations between them, they all share a common N-terminal sequence (Met-Glu-Asp) that differs from mammalian enzymes.

The molecular masses of all SERCA type Ca^{2+} transport ATPases of muscle are close to 110 kDa. Their N-terminal sequences are similar: Met-Glu-X(Ala, Asn, Glu, Asp)-X (Ala, Gly, Ile). The Met-Glu-X-X sequence serves as signal for the acetylation of N-terminal methionine both in soluble and in membrane proteins (Tong, 1977; 1980).

THE PREDICTED TOPOLOGY OF Ca^{2+}-ATPases

Combining structural and biochemical information, MacLennan and his colleagues constructed a hypothetical model of the tertiary structure of Ca^{2+}-ATPase (MacLennan *et al.*, 1985; 1997) that had interesting mechanistic implications (Fig. 1), and was largely confirmed by recent structural data (MacLennan & Green, 2000; Toyoshima *et al.*, 2000; Green *et al.*, 2002; Toyoshima & Nomura, 2002; Toyoshima *et al.*, 2003). The structure was divided into three major parts, designated as the cytoplasmic headpiece, the stalk domain and the transmembrane domain. Only short loops were assumed to be exposed on the luminal side of the membrane.

More than half of the total mass of the ATPase molecule is exposed on the cytoplasmic surface of the membrane, forming the cytoplasmic head piece (Fig. 1). The headpiece contains six subdomains: the N-terminal re-

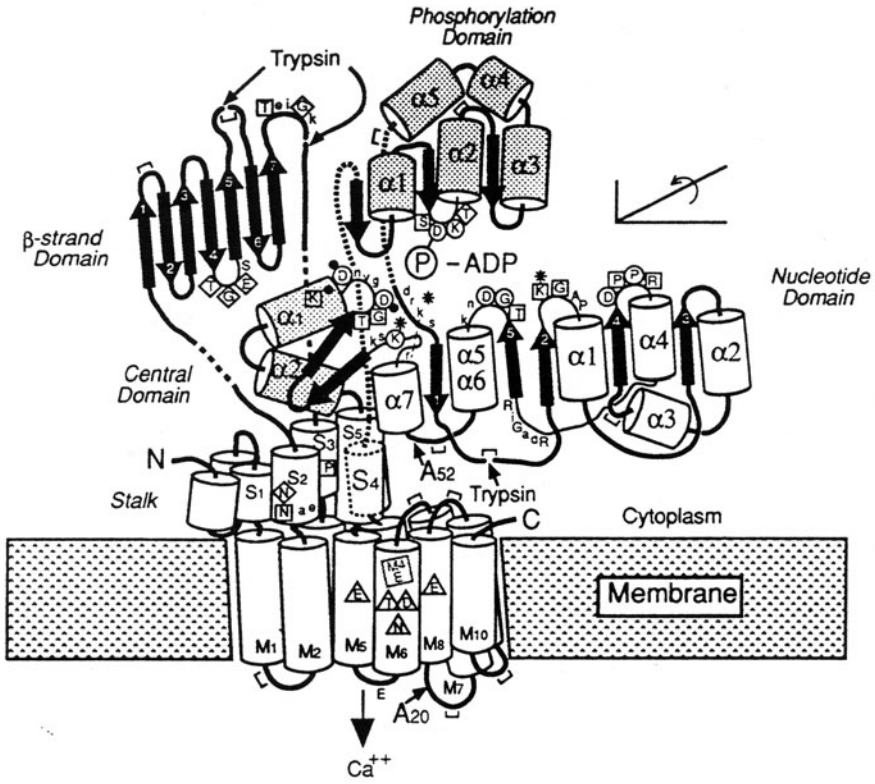

Figure 1. Model of the Ca^{2+} transport ATPase of sarcoplasmic reticulum.

The diagram shows the approximate relationships between secondary structure elements within domains and a possible set of relationships between domains. α-Helical segments are represented as cylinders, and β-strands as arrows. The stalk helices are marked S and the transmembrane segments as M. For clarity, the stalk segments 2, 3, and 4 are linked by dashed connections of arbitrary length to the main cytoplasmic domains. An arrangement consistent with the lobes present in three-dimensional reconstructions is obtainable by rotating the major cytoplasmic region about the axis indicated in the upper right. This brings the phosphorylation and central hinge domains (shaded) behind the nucleotide domain and into close proximity with the stalk. The ATP binding cleft would be approximately in the plane of the paper and the first trypsin cleavage site (trypsin 1), and the A_{52} antibody site would be exposed on the surface. The β-strand, or B domain, could be positioned so that the conserved TGES loop is near the cleft, which would be consistent with the effects of vanadate on this domain. The positions of 13 sites at which insertions or deletions are observed are indicated by •. Sites of mutations in the calcium pump that affect activity are widely distributed but are confined to well-conserved sites. The sequences of these regions and the effects of mutations are shown. Five main types were distinguishable: (1) No effect, X (only a few of the 150 sites are shown); (2) decreased Ca^{2+} transport, ¤; (3) no transport, but normal phosphorylation implying that the step $E_1P \rightarrow E_2P$ is blocked, ◊; (4) no Ca^{2+} control of phosphorylation, Δ; and (5) no transport, no phosphorylation, 0. Some nonmutated residues, shown in lower case, are included to provide context for the mutants. The residues (*) modified by affinity labels of the Ca^{2+} pump are all lysines (K), which, from left to right, are labeled by ATP.PAL/ Ca^{2+}, ATP.PAL/EGTA, FITC. Sites that are labeled in the Na^+,K^+ATPase (●) are FSBA(K), CIR.ATP(D). The secondary trypsin cleavage site(s) are shown as trypsin 2. The position of ATP between the phosphorylation and nucleotide domain is indicated with the terminal phosphate next to Asp351 that serves as phosphate acceptor. Mutations in the stalk sector and in the periphery of transmembrane domain had little effect on Ca^{2+} transport. The binding site for antibody A_{20} is on the luminal surface. Printed with permition from Green & Stokes (1992).

gion (residues 1–40), the strand domain (residues 131–238), the phosphorylation domain (residues 328–505), the nucleotide binding domain (residues 505–680), the hinge domain (residues 681–738), and the C-terminal region (residues 902–). The phosphorylation and nucleotide binding domains (residues 328–680) form the active site of ATP hydrolysis and are closely related structurally and functionally.

The stalk region (S1–S5) connects the headpiece to the membrane (Fig. 1). In the early models of the enzyme, the eighteen glutamic acid and three aspartic acid residues in the stalk helices (S1–S5) were considered to form the high affinity binding site for Ca^{2+} at the entrance to the putative Ca^{2+} transport channel. The low affinity Ca^{2+} binding sites were tentatively assigned to the cluster of four glutamic acid residues located in a loop between transmembrane helices M1 and M2 on the lumenal side of the membrane. However mutagenesis of the acidic or amidated amino -acid residues in the stalk region or in the lumenal loop had little or no effect on ATP-dependent Ca^{2+} transport or on enzyme phosphorylation, and the Ca^{2+} binding sites were eventually located in the transmembrane domain.

The intramembranous part of the molecule (the transmembrane domain) was predicted to contain ten hydrophobic transmembrane helices (M1–M10) that anchor the Ca^{2+}-ATPase to the lipid bilayer and form the transmembrane channel for the passage of Ca^{2+} (Toyoshima *et al.*, 2000) (Fig. 1). Both the N- and the C-terminal segments of the SERCA1 Ca^{2+}-ATPase are exposed on the cytoplasmic surface of the membrane, while the loop containing residues 877–888 is on the lumenal surface. The extended tail section of SERCA2b may form an additional eleventh transmembrane domain, locating its C-terminus on the lumenal surface.

THE STRUCTURE AND INTERACTIONS OF Ca^{2+}-ATPase DETERMINED BY ELECTRON CRYSTALLOGRAPHY

Early observations

The Ca^{2+}-ATPase of SR was first visualized by negative staining with uranyl acetate or K-phosphotungstate in the form of 40 Å diameter surface particles, that were attached to the membrane by a narrow stalk (Ikemoto *et al.*, 1968; Martonosi, 1968). Freeze-etch electron microscopy revealed 85 Å diameter intramembranous particles, that were more numerous in the cytoplasmic than in the lumenal fracture face of the membrane (Baskin & Deamer, 1969). These early observations established that the Ca^{2+}-ATPase consists of a cytoplasmic domain, connected by a stalk to an intramembrane domain, and that the disposition of Ca^{2+}-ATPase in the membrane plane is asymmetric, with much of its mass on the cytoplasmic surface and within the cytoplasmic leaflet of the bilayer.

Both in native SR and in reconstituted Ca^{2+}-ATPase preparations the average density of 40 Å surface particles (20 000–30 000/μm^2) was about four times greater than that of the intramembrane particles (4500–7000/μm^2) leading to the suggestion that the 85 Å particles represent the membrane domains of ATPase oligomers consisting on the average of four ATPase molecules (Jilka *et al.*, 1975; Franzini-Armstrong & Feguson, 1985). Association between ATPase molecules was also observed by fluorescence energy transfer measurements on native and reconstituted membranes (Vanderkooi *et al.*, 1977; Papp *et al.*, 1987), and by exclusion chromatography on detergent solubilized preparations (Andersen, 1989). These observations indicate a tendency of the Ca^{2+}-ATPase to form oligomers, although the functional significance of these associations remains still ill-defined.

Crystallization of Ca^{2+}-ATPase in various conformations

The tendency for ATPase–ATPase interactions becomes particularly pronounced when the Ca^{2+}-ATPase is stabilized by ligands in the E_1 or E_2 conformation. Under these conditions extensive arrays of ATPase crystals form within native SR membranes or in systems containing solubilized or purified Ca^{2+}-ATPase, that have distinct morphology

depending on crystallization conditions. Three distinct crystal forms of the Ca^{2+}-ATPase have been developed (Taylor *et al.*, 1988a; Martonosi *et al.*, 1991; Martonosi, 1992, 1995) (Fig. 2).

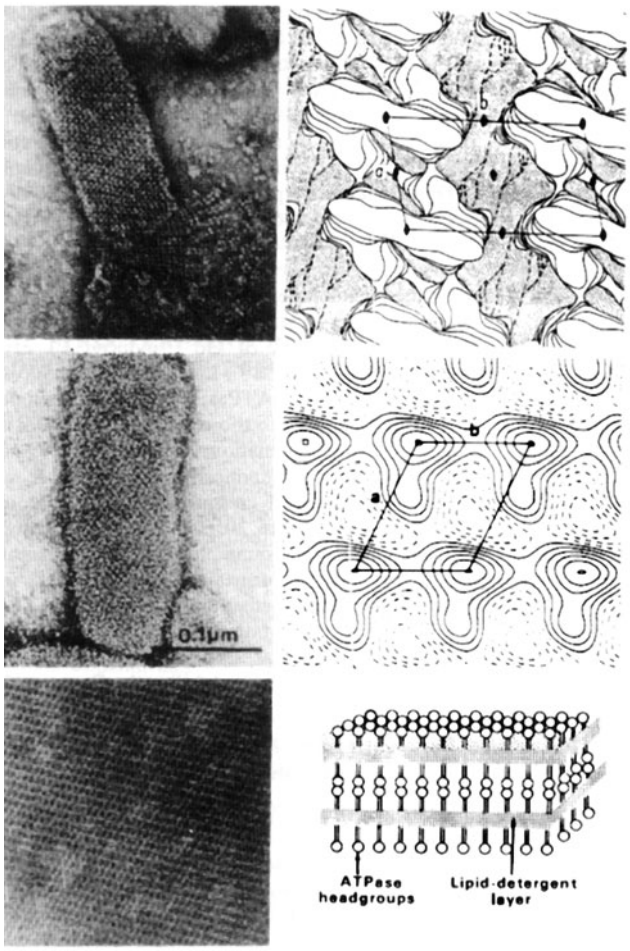

Figure 2. The interactions between ATPase molecules in projection maps of three distinct Ca^{2+}-ATPase crystals.

Top panels. E_2vanadate crystals induced by vanadate in a Ca^{2+}-free medium. Dimer chains of pear-shaped ATPase molecules wind diagonally around the crystalline tubules. Osmotic lysis occasionally separates individual dimer chains (top left). The two ATPase molecules within the dimers are in antiparallel arrangement, held together by massive bridges; these are marked by the corners of the dimeric unit cells in the projection map (top right). The dimers form dimer chains by interactions between the lobes and the heads of adjacent ATPase molecules. The stippled area represents the cytoplasmic surface of the bilayer and the broken lines indicate positive densities that connect the dimer chains within the bilayer. **Middle panels**. E_1 type Ca^{2+}-ATPase crystals induced by praseodymium. The structural units of the E_1 crystals are ATPase monomers arranged in a parallel orientation, and their interactions are distinct from those seen in E_2vanadate crystals. **Bottom panels**. Ca^{2+}-induced ATPase crystals in detergent solutions. The Ca^{2+}-ATPase molecules project symmetrically from both sides of the bilayer and interact with ATPase molecules in adjacent lamellae. From Martonosi (1995).

Dimeric tubular crystals are induced by vanadate or inorganic phosphate in a Ca^{2+}-free medium; these are assumed to represent the E_2 conformation of the Ca^{2+}-ATPase (Dux & Martonosi, 1983a, 1983c; 1984; Taylor *et al.*, 1984; 1988a; 1988b) (Fig. 2 top panels). Monomeric tubular crystals are induced by μmolar calcium or lanthanides at pH 8.0; these are assigned to the E_1 state (Dux *et al.*, 1985) (Fig. 2 middle panels). Both dimeric or monomeric tubular crystals readily form in native or reconstituted SR vesicles. These two crystal forms can be reversibly interconverted by changing the ionic composition or membrane potential (Dux & Martonosi, 1983d; Beeler *et al.*, 1984; Dux *et al.*, 1985b; Jona & Martonosi, 1986). Since the $E_1 \rightarrow E_2$ transition does not involve changes in the circular dichroism spectrum of the Ca^{2+}-ATPase (Csermely *et al.*, 1987), the structural differences between these two states were suggested to arise by sliding motions of domains rather than by a rearrangement of the secondary structure of the protein. Detergent-solubilized Ca^{2+}-ATPase forms multilamellar crystals at pH 6.0 and 10–20 mM Ca^{2+} concentration (Dux *et al.*, 1987; Pikula *et al.*, 1988; Taylor *et al.*, 1988b; Misra *et al.*, 1991; Varga *et al.*, 1991) (Fig. 2 bottom panels). The conformational assignment of this crystal form is uncertain because the low pH and very high Ca^{2+} concentration produces structural effects (Arrondo *et al.*, 1987) that do not occur under physiological conditions and are distinct from the properties of kinetically defined E_1Ca_2 state.

The characteristics of these three crystal forms will be discussed in turn.

The vanadate-induced tubular E_2 crystals

Vanadate ions or inorganic phosphate in the absence of calcium shift the conformational equilibrium of Ca^{2+}-ATPase toward the E_2 state and induce the formation of P2 type Ca^{2+}-ATPase crystals with Ca^{2+}-ATPase dimers as structural units (Dux & Martonosi, 1983a; 1983b; 1984; Taylor *et al.*, 1984; 1986a; 1986b) (Fig. 2 top panels). The unit cell dimensions are a – 65.9 Å; b – 114.4 Å and γ – 77.9 Å (Taylor *et al.*, 1984). The vanadate-induced Ca^{2+}-ATPase crystals are disrupted by increasing the Ca^{2+} concentration of the medium to 0.1–10 mM (Dux & Martonosi, 1983c).

The vanadate-induced E_2 type crystals consist of chains of Ca^{2+}-ATPase dimers (Fig. 2, top panels) wound in a righthanded helix around the cylindrical tubules of 600–900 Å diameter. These dimer chains were observed by negative staining (Taylor *et al.*, 1984; 1986a), freeze-fracture (Peracchia *et al.*, 1984; Ting-Beall *et al.*, 1987), freeze-drying and rotary shadowing (Ferguson *et al.*, 1985; Franzini-Armstrong & Ferguson, 1985), and in frozen-hydrated specimens (Taylor *et al.*, 1986b). Occasionally the helical lattice unwinds revealing isolated chains of ATPase dimers separated from neighboring dimer-chains by variable distances (Dux & Martonosi, 1983c).

The cylindrical geometry of crystalline tubules is determined by the forces of the ATPase–ATPase interactions (Varga & Martonosi, 1992). During the crystallization of Ca^{2+}-ATPase in giant spherical vesicles of 1–25 μm diameter, long crystalline ridges develop separated by deep furrows; as the crystallization proceeds the ridges eventually pinch off and close into long crystalline cylinders of 600–900 Å diameter with a curvature that is consistent with the geometry of ATPase–ATPase interactions. We assume that the conversion of spherical into longitudinal SR in developing muscle, that follows the accumulation of Ca^{2+}-ATPase in the membrane (Boland *et al.*, 1974; Tillack *et al.*, 1974; Martonosi 2000), may also reflect the influence of ATPase molecules on membrane shape.

Three-dimensional reconstruction of the structures of vanadate-induced Ca^{2+}-ATPase crystals preserved in uranyl acetate yielded an image of the cytoplasmic region of the molecule at 20–25 Å resolution (Taylor *et al.*, 1986a). In the view normal to the membrane plane, each map shows pear-shaped densities arranged in antiparallel strands (Fig. 2, top panels) that correspond to the ribbons of Ca^{2+}-ATPase dimers. The Ca^{2+}-ATPase molecules extend about 60 Å above the surface of the bilayer, and their profiles are 65 Å long in a direction parallel to the "a" axis of the crystal and about 40 Å wide in the direction of the "b" axis. The only visible cytoplasmic connection between the two molecules that make up the Ca^{2+}-ATPase dimers is a 17 Å thick bridge that crosses the intradimer gap at a height of 42 Å above the surface of the bilayer (Taylor *et al.*, 1986a). The cytoplasmic domains reconstructed from negatively stained (Taylor *et al.*, 1986a) and from frozen-hydrated rabbit (Taylor *et al.*, 1986b) and scallop (Castellani *et al.*, 1985) SR have similar shapes.

Cryo-electron microscopy and helical reconstruction at 14 Å resolution (Toyoshima *et al.*, 1993) confirmed the pear-shaped profile of the cytoplasmic domain and revealed four distinct segments (A1, A2, B, C) in the transmembrane domain of Ca^{2+}-ATPase. These were tentatively assigned to transmembrane helices M2–M5 (A_1), M6, M8 (A2), M7 (B) and M1, M10 (C), respectively. The small lumenal mass was assigned to the M7–M8 loop (Toyoshima *et al.*, 1993). At 8 Å resolution the pear-shaped cytoplasmic domain emerged in greater detail and densities corresponding to all ten transmembrane segments could be seen (Zhang *et al.*, 1998), but the identification of these densities with the transmem-

brane helices M1–M10 still remained speculative.

CrATP, an inhibitor of Ca^{2+}-ATPase, forms a stable complex with the ATP-binding site of the enzyme, leading to the occlusion of 2 Ca^{2+} in a nonexchangeable form in the enzyme, with inhibition of ATP hydrolysis and Ca^{2+} transport (Serpersu *et al.*, 1982; Vilsen & Andersen 1992; Vilsen, 1995). The bound Ca^{2+} is slowly released from the enzyme in the presence of EGTA, while CrATP remains firmly attached to its binding site (Coan *et al.*, 1994; Vilsen, 1995). The CrATP complex of Ca^{2+}-ATPase was crystallized by vanadate in a Ca^{2+}-free medium (Stokes & Lacapere, 1994), and the crystals have been analyzed by cryo-electron microscopy to determine the location of the ATP-binding site (Yonekura *et al.*, 1997). Comparison of the three-dimensional maps of Ca^{2+}-ATPase crystals obtained with or without CrATP showed a highly significant density difference corresponding to a groove on the lower surface of the "beak" of the cytoplasmic domain. This area was resolved as a 20 × 10 × 7 Å hole of low density in the absence of CrATP that became filled when CrATP was present, suggesting that it corresponds to the ATP-binding site. This site is located about 43 Å above the surface of the membrane (Yonekura *et al.*, 1997) in agreement with the 40–60 Å distance between the ATP-binding site and the phospholipid-water interface determined by fluorescence energy transfer (Bigelow & Inesi, 1992). There were no significant density differences attributable to CrATP binding in other regions of the Ca^{2+}-ATPase.

The assignment of the vanadate and inorganic phosphate induced tubular crystals to the E_2 conformation of Ca^{2+}-ATPase is supported by the observation that Ca^{2+} at micromolar concentration prevents (Dux & Martonosi, 1983c), while thapsigargin promotes their formation (Stokes & Lacapere, 1994). ATP (1 mM), ADP, AMPPCP, AMPPNP (Dux & Martonosi, 1983c) and CrATP (Stokes & Lacapere, 1994) that interact with both conformations of Ca^{2+}-ATPase, had no effect on crystallization. Decavanadate, that may also serve as an ATP analogue (Csermely *et al.*, 1985a; 1985b; Varga *et al.*, 1985; Coan *et al.*, 1986), is the vanadate species generally used to induce crystallization. Some of the decavanadate sites of the Ca^{2+}-ATPase are blocked by reaction of Lys515 with fluorescein-5′-isothiocyanate (FITC), accompanied by inhibition of ATP binding (Csermely *et al.*, 1985a; 1985b; Varga *et al.*, 1985). As reaction of Lys515 with FITC does not affect the crystallization of Ca^{2+}-ATPase by mono- or decavanadate, the vanadate site blocked by FITC is not required for crystallization (Csermely *et al.*, 1985a; 1985b; Varga *et al.*, 1985; Xu *et al.*, 2002).

Phospholamban, a Ca^{2+}-dependent inhibitor of Ca^{2+}-ATPase, was reconstituted at various molar ratios with the Ca^{2+}-ATPase, and tubular cocrystals were formed in a crystallization medium of 0.1 M KCl, 20 mM imidazole, pH 7.0, 5 mM $MgCl_2$, 0.5 mM EGTA, 0.5 mM Na_3VO_4, and various amounts of thapsigargin (Young *et al.*, 2001). The structure of Ca^{2+}-ATPase at 8–10 Å resolution was unaffected by the presence of phospholamban, suggesting that the inhibition of ATPase activity and Ca^{2+} transport by phospholamban may be due to the inhibition of the domain movements of Ca^{2+}-ATPase that accompany Ca^{2+} transport.

The cryo-electron microscopic structures of renal Na^+,K^+-ATPase obtained from frozen-hydrated vanadate-induced E_2V type crystals at 9.5–11.0 Å resolution (Hebert *et al.*, 2001; Rice *et al.*, 2001) show considerable similarity with the structure of Ca^{2+}-ATPase, but there are also differences partly due to the presence of the β and γ subunits in the Na^+,K^+-ATPase.

Crystallization of Ca^{2+}-ATPase by Ca^{2+} and lanthanides

The Ca^{2+}-ATPase was also crystallized in rabbit SR vesicles in a medium of 0.1 M KCl, 10 mM imidazole, pH 8, and 5 mM $MgCl_2$ by

the addition of either $CaCl_2$ (100 μM) or lanthanide ions (1–8 μM) that stabilize the E_1 conformation of the enzyme (Martonosi *et al.*, 1991; Martonosi, 1995; Dux *et al.*, 1985b; Ting-Beall *et al.*, 1987). After incubation at 2°C for 5 to 48 h, crystalline arrays were observed on the surface of about 10–20% of the vesicles in SR preparations obtained from fast-twitch rabbit skeletal muscles. The crystals induced at micromolar Ca^{2+} concentration are likely to represent the E_1Ca_2 state stabilized by Ca^{2+} binding to the two high affinity sites of the Ca^{2+}-ATPase.

Analysis of the lanthanide-induced crystalline arrays by negative staining (Dux *et al.*, 1985b) or freeze-fracture electron microscopy (Ting-Beall *et al.*, 1987) reveals obliquely oriented rows of particles, corresponding to individual Ca^{2+}-ATPase molecules (Fig. 2, middle panels). The unit cell dimensions for the gadolinium-induced Ca^{2+}-ATPase crystals are a = 61.7 Å, b = 54.4 Å, and γ = 111. Similar cell constants were obtained for the crystals induced by lanthanum, praseodymium and calcium (Dux *et al.*, 1985b). The unit cell dimensions of the E_1 crystals are consistent with a single Ca^{2+}-ATPase monomer per unit cell. The space group of the E_1 type crystals is P1 (Dux *et al.*, 1985b), while that of the E_2 crystals is P2 (Taylor *et al.*, 1984; 1986a; 1988a; Martonosi *et al.*, 1991). At the relatively low resolution (about 20 Å) that is currently available, the projected pear-shaped profiles of the cytoplasmic domains of ATPase molecules appear similar in the E_1 and E_2 type crystals; however, the pattern of ATPase–ATPase interactions revealed by these crystals is clearly different, and analysis at higher resolution is likely to reveal structural differences.

CrATP, a suicide inhibitor of Ca^{2+}-ATPase, that arrests the enzyme in a Ca^{2+}-occluded E_1 state (Serpersu *et al.*, 1982; Vilsen & Andersen, 1992; Vilsen 1995), produced E_1 type crystals very similar to those obtained with calcium or lanthanides (Dux *et al.*, 1985b). These observations support the assignment of the P1 type crystals to the E_1 conformation of the Ca^{2+}-ATPase. After chelation of Ca^{2+} with EGTA and addition of vanadate, the E_1 type crystals are reversibly converted into the E_2 form (Dux *et al.*, 1985b). Stabilization of E_1 state by inside negative membrane potential imposed by ion substitution accelerated the formation of E_1(P1) type crystals and destabilized the E_2(P2) crystals (Dux & Martonosi, 1983d; Beeler *et al.*, 1984; Dux *et al.*, 1985b; Jona & Martonosi, 1986). Inside positive membrane potential had the opposite effect.

The assignment of the vanadate- and P_i-induced tubular crystals to the E_2 conformation and the Ca^{2+}- and lanthanide-induced tubular crystals to the E_1 conformation is further supported by partial proteolysis profiles (Dux *et al.*, 1985a; 1985b; Dux & Martonosi, 1983b; Andersen & Jorgensen, 1985), and by fluorescence data using protein tryptophan and covalently bound FITC as reporter groups (Jona & Martonosi, 1986). Some uncertainty is introduced into these assignments by the observation that under certain conditions lanthanides can bind to the Ca^{2+}-ATPase at sites distinct from the high affinity Ca^{2+} binding sites (Highsmith & Head, 1983; Ogurusu *et al.* 1991) and may stabilize the E_2 state (Girardet *et al.* 1989). As yet no high resolution structure is available of this crystal form, in spite of its obvious relevance to the E_1Ca_2 state.

Calcium-induced crystallization of Ca^{2+}-ATPase in detergent-solubilized sarcoplasmic reticulum

Further advance toward a high resolution structure of Ca^{2+}-ATPase was achieved by production of three-dimensional crystals of sufficient size and quality for X-ray diffraction analysis. Since the detergent-solubilized Ca^{2+}-ATPase is notoriously unstable, the first task was to find conditions that preserve the

ATPase activity of the solubilized enzyme. By systematically testing several hundred conditions, it has been found (Pikula *et al.*, 1988; Taylor *et al.*, 1988b) that the Ca^{2+}-modulated ATPase activity was preserved for several months at 2°C under nitrogen in a crystallization medium of 0.1 M KCl, 10 mM K-Mops, pH 6.0, 3 mM $MgCl_2$, 3 mM NaN_3, 5 mM dithiothreitol, 25 IU/ml Trasylol, 2 μg/ml 1,6-di-*tert*-butyl-*p*-cresol, 20 mM $CaCl_2$, 20% glycerol, 2 mg/ml SR protein, and 4–8 mg/ml of the appropriate detergent, such as $C_{12}E_8$, Brij 36T, Brij 56, or Brij 96 (Pikula *et al.*, 1988; Taylor *et al.*, 1988b). After incubation for 6–10 days under nitrogen, ordered crystalline arrays of Ca^{2+}-ATPase appeared that increased in number and size during the next several weeks. The microcrystals formed in the presence of 20 mM Ca^{2+} and 20% glycerol contain highly ordered crystalline sheets of Ca^{2+}-ATPase molecules, that associate into multilamellar stacks (Fig. 2, bottom panels) consisting frequently of more than 100 layers (Dux *et al.*, 1987; Pikula *et al.*, 1988; Taylor *et al.*, 1988b). The formation of multilamellar arrays is optimal at low temperature; at 25°C the crystals rapidly disintegrate, but can be reformed again by lowering the temperature to 2°C.

Two distinct patterns of repeats were observed that represent different projections of the structure (Martonosi *et al.* 1991; Martonosi, 1995; Dux *et al.* 1987; Taylor *et al.* 1988b). In the first view, layers of densities are seen that repeat at about 103–147 Å in sectioned specimens, at 130–170 Å in negatively stained material, and at 170–180 Å in images of frozen-hydrated crystals (Taylor *et al.* 1988b). These layered structures represent side-views of stacked multilamellar arrays of ATPase molecules. The about 40 Å thick stain-excluding core of the lamellae contains a lipid-detergent phase into which the hydrophobic tail portions of the ATPase molecules are inserted symmetrically on both sides (Taylor *et al.* 1988b). The periodicity of the lamellae is defined by contacts between the hydrophilic headgroups of the ATPase molecules. The 170 Å spacing of the layers seen in frozen hydrated specimens is consistent with the dimensions of the ATPase molecules, suggesting minimal interdigitation between the cytoplasmic domains of Ca^{2+}-ATPase that interact from adjacent lamellae (Taylor *et al.* 1988b). The interactions between the exposed headgroups are responsible for the association of lamellae into Type I three-dimensional structures. The high Ca^{2+} concentration (about 20 mM), low temperature (about 2°C) and the low pH (about 6.0) required for crystallization presumably promote these interactions.

In the second view of the three-dimensional crystals, the projected image normal to the plane of the lamellae (Fig. 2, bottom panels) shows ordered arrays of 40–50 Å diameter particles with two sets of periodicity of about 50 Å and 80 Å, respectively; these particles represent the cytoplasmic domains of ATPase molecules (Taylor *et al.* 1988b). Taylor *et al.* (1988b) suggested that the crystals belong to the two-sided plane group C12, in which there are four ATPase molecules per unit cell of 9113 $Å^3$, with ATPase dimers related by a two-fold rotational axis within the membrane plane parallel to the b cell axis. While the arrangement of ATPase molecules was highly ordered within each sheet, there was a slight rotational misalignment between the successive layers in the stacks, that prevented the separation of the projections of individual layers (Taylor *et al.* 1988b). Stokes & Green (1990a; 1990b) confirmed the C12 symmetry, but they found ordered stacking in the third dimension, leading to the conclusion that the crystals belonged to the three-sided space group C2. The four ATPase molecules occupy about 35% of the unit cell, leaving the remainder of space for lipids and detergents. The crystals diffracted to 7.2 Å in X-ray powder patterns and to 4.1 Å in electron diffraction.

The crystallization procedure developed for SR Ca^{2+}-ATPase (Pikula *et al.*, 1988; Taylor *et al.*, 1988b) has also been used with appropri-

ate modification of the ionic conditions for the preparation of multilamellar crystals of the pig kidney Na^+,K^+-ATPase (Varga, 1993; Taylor & Varga, 1994; Varga & Szabolcs, 1994), pig and rabbit stomach H^+,K^+-ATPase (Varga, 1994), and pig erythrocyte plasma membrane Ca^{2+}-ATPase (Pikula *et al.*, 1991).

The detergent-solubilized Ca^{2+}-ATPase required high (10–20 mM) Ca^{2+} concentration for crystallization (Pikula *et al.*, 1988; Taylor *et al.*, 1988b) presumably due to Ca^{2+} binding to low affinity Ca^{2+} binding sites. No multilamellar crystals were obtained at submillimolar Ca^{2+} concentrations that stabilize the kinetically defined E_1Ca_2 state associated with Ca^{2+}-binding to the two high affinity Ca^{2+} binding sites of the calcium ATPase. Furthermore, raising the Ca^{2+} concentration from 0.1 mM to 10–20 mM caused the appearance of an infrared peak at 1650 cm^{-1}, that is absent in the E_1Ca_2 state stabilized by 0.1 mM Ca^{2+} (Arrondo *et al.*, 1987). These observations suggest that the high Ca^{2+} concentrations (10–20 mM) required for the production of multilamellar Ca^{2+}-ATPase crystals induce secondary effects on the structure of Ca^{2+}-ATPase, making the conformational assignment to the kinetically defined E_1Ca_2 state (Toyoshima *et al.*, 2000) doubtful.

Electron crystallography of multilamellar Ca^{2+}-ATPase crystals

The crystallographic analysis of Ca^{2+}-induced multilamellar crystals containing stacks of 2 two-dimensional arrays presents technical problems related both to specimen preparation and to data analysis (Michel, 1990). To overcome these difficulties a major effort was launched during the last decade to improve specimen preparation by decreasing stacking and increasing the area of crystals through changes in lipid : detergent ratio (Lacapere *et al.*, 1998; Cheong *et al.*, 1996), the use of higher glycerol concentration and lower temperature (Varga *et al.*, 1991; Shi *et al.*, 1995), and by replacing 0.1 M KCl with 0.8 M Na-propionate in the crystallization medium (Misra *et al.*, 1991). There were also advances in data collection and analysis (Shi *et al.*, 1998). This led to a projection map of Ca^{2+}-ATPase at 9 Å resolution from Ca^{2+}-induced multilamellar crystals (Ogawa *et al.*, 1998), and its comparison with the projection map of the Ca^{2+}-ATPase obtained earlier from vanadate-induced tubular Ca^{2+}-ATPase crystals (Toyoshima *et al.*, 1993; Zhang *et al.*, 1998). A conspicuous feature of the Ca^{2+}-induced structure is that the cytoplasmic domain consists of two well-separated densities (designated as HL and HS domains). The large HL domain contains two subdomains of nearly equal density that are connected to the transmembrane domain by a thin rod. The small HS domain has only weak connection with the HL or transmembrane domains. The transmembrane domain contains three columns of densities, all inclined about 30° from the normal of the bilayer plane. The split appearance of the cytoplasmic domain in Ca^{2+}-induced crystals (Ogawa *et al.*, 1998) is in marked contrast to the condensed pear-shaped structure seen in vanadate-induced tubular crystals (Toyoshima *et al.*, 1993; Zhang *et al.*, 1998). The largest change is seen around the groove on the lower surface of the beak (Ogawa *et al.*, 1998), that was earlier identified as the ATP binding pocket of Ca^{2+}-ATPase (Toyoshima *et al.*, 1993; Yonekura *et al.*, 1997). The stalk segment shifts from the left to the right of the headpiece in Ca^{2+}-induced multilamellar crystals, and translational movements together with a change in inclination of transmembrane helices were seen in the transmembrane domain (Ogawa *et al.*, 1998).

These structural differences between Ca^{2+}-free and Ca^{2+}-ligated enzyme forms are consistent with the large structural changes seen in earlier X-ray diffraction studies on lamellar arrays of SR vesicles (DeLong *et al.*, 1993).

THREE DIMENSIONAL STRUCTURE OF SERCA1a BY X-RAY CRYSTALLOGRAPHY

Ca^{2+}-ATPase structure in the Ca^{2+}-bound state

The three-dimensional structure of Ca^{2+}-ATPase was determined at 2.6 Å resolution (Fig. 3) by X-ray crystallography of the Ca^{2+}-mixture of purified Ca^{2+}-ATPase with phosphatidylcholine against a buffer of 0.8 M Na-butyrate, 2.7 M glycerol, 10 mM $CaCl_2$, 3 mM $MgCl_2$, 2.5 mM sodium azide, 0.2 mM dithiothreitol, and 20 mM Mes, pH 6.1. All 994 amino-acid residues were identified together with 250 water molecules in the cytoplasmic and lumenal regions and 30 water molecules in the transmembrane domain. The high resolution structure largely confirms earlier predictions based on the amino-acid sequence (MacLennan *et al.*, 1985; 1997; Brandl *et al.*, 1986; Andersen, 1995; Moller *et al.*,

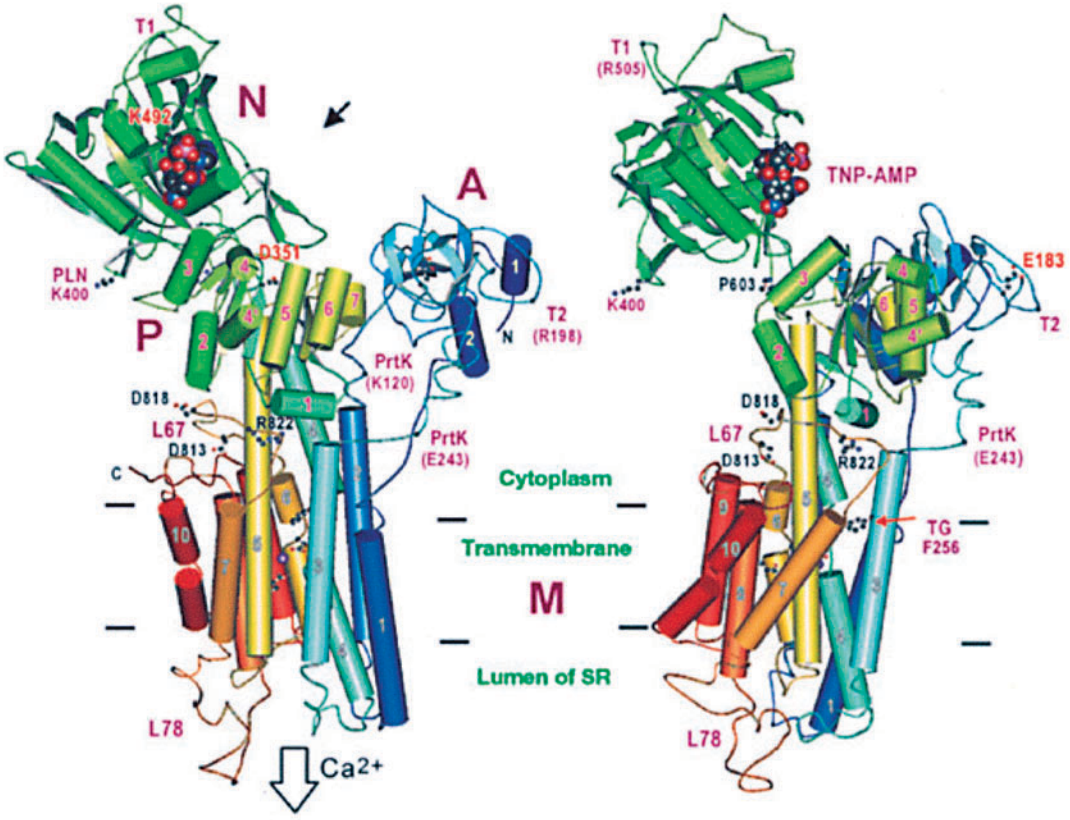

Figure 3. Architecture of the sarcoplasmic reticulum Ca^{2+}-ATPase based on X-ray crystallography of multilamellar Ca^{2+}-ATPase crystals induced by Ca^{2+}.

α-Helices are represented as cylinders and β-strands as arrows. Cylinders are not used for one turn helices. Three cytoplasmic domains are labelled (A, N and P). Transmembrane helices (M1–M10) and those in domains A and P are numbered. The model is orientated so that transmembrane helix M5 is parallel to the plane of the paper. The model in the right panel is rotated by 50° around M5. The M5 helix is 60 Å long and serves as a scale. Several key residues are shown in ball-and-stick, and TNP-AMP by CPK. D351 is the residue of phosphorylation. Two spheres represent Ca^{2+} in the transmembrane binding sites. The binding sites for phospholamban (PLN) and thapsigargin (TG) are marked as are major digestion sites for trypsin (T1 and T2) and proteinase K (PrtK). Figure prepared with MOLSCRIPT. Modified from Toyoshima *et al.* (2000). Printed with permission from Nature Publishing Group.

induced multilamellar Ca^{2+}-ATPase crystals (MacLennan & Green, 2000; McIntosh, 2000; Toyoshima *et al.*, 2000) formed by dialysing a

1996), and electron crystallography (Ogawa *et al.*, 1998), but also reveals significant new features in several regions of the molecule. The cytoplasmic headpiece is clearly separated into three distinct structures (Fig. 3), designated as the P, N and A domains.

The phosphorylation or P domain contains Asp351, the site of autophosphorylation by ATP. It is composed of an N-terminal part (residues 330–359), that is connected to transmembrane helix M4 and a C-terminal part (residues 605–737) that is linked to transmembrane helix M5. The nucleotide binding N domain (residues 360–604) is nestled between these two segments. The P domain is assembled into a seven-strand parallel β-sheet with eight short helixes that form a typical Rossman-fold. Aspartate 351 is located at the C-terminal end of the central β strand, surrounded by the amino acids required for the hydrolysis of ATP (Fig. 3). The structure is analogous to the core domain of L-2 haloacid dehydrogenase (Aravind *et al.*, 1998; Stokes & Green, 2000). The surface is negatively charged.

The nucleotide-binding N domain (residues 360–604) inserted between the two segments of the P domain, is formed by a seven strand antiparallel β-sheet between two helix bundles (Fig. 3). Soaking the crystals in a solution of 2′,3′-*O*-(2,4,6-trinitrophenyl)AMP (TNP-AMP) permitted the localization of the ATP-binding sites within the N domain near Phe487, Lys515, and Lys492, that are known to be involved in ATP-binding (Andersen, 1995). Arg560 and Thr441, two newly identified components of the ATP binding site, are also in the vicinity. Lys492 can be covalently labeled with 8-azido-2′,3′-*O*-(2,4,6-trinitrophenyl)ATP (8-azido-TNP-ATP) and other ATP derivatives (McIntosh *et al.*, 1992; McIntosh & Woolley 1994; Andersen, 1995; Moller *et al.*, 1996; McIntosh, 1998), and reaction of Lys515 with FITC decreases the affinity of ATP-binding by several orders of magnitude (Pick, 1981). The ATP binding pocket is positively charged in contrast to the negative charge of the P domain surface.

ATP accelerates several steps of Ca^{2+} transport following phosphorylation causing a secondary activation of ATP hydrolysis at high ATP concentration. Attempts were made to explain this effect by ATP-binding at a single site or at two distinct sites. The observation of a single binding site for TNP-AMP (Toyoshima *et al.*, 2000) tends to favor a mechanism in which binding of ATP to the catalytic site accounts for the complex ATP dependence (McIntosh, 2000). However, the problem is not fully settled (MacLennan & Green, 2000) as the binding site of TNP-AMP identified in Ca^{2+}-induced multilamellar crystals (Toyoshima *et al.*, 2000) appears to be at some distance from the binding site of CrATP in the tubular crystals induced by vanadate in the absence of Ca^{2+} (Zhang *et al.*, 1998; Yonekura *et al.*, 1997; Ogawa *et al.*, 1998). Furthermore, the formation of multilamellar crystals was inhibited by CrATP and prevented by other ATP analogues such as AMPPCP (Stokes & Lacapere, 1994), that did not interfere with the formation of tubular Ca^{2+}-ATPase crystals. These observations imply that the structure and location of the ATP-binding site may be influenced by enzyme conformation and/or the crystallization conditions.

By fitting the atomic model (Toyoshima *et al.*, 2000) to the 8 Å map of Ca^{2+}-ATPase from vanadate-induced tubular crystals (Zhang *et al.*, 1998), a region of high density was seen at a positively charged groove formed by the N and P domains. This density was attributed to decavanadate bound to the Ca^{2+}-ATPase (Toyoshima *et al.*, 2000). The decavanadate-binding site is surrounded by positively charged amino-acid residues, Arg489, Lys492 and Arg678, and it is close to Asp351. The decavanadate-binding site is formed by rearrangement of the cytoplasmic domains of Ca^{2+}-ATPase in which domain A undergoes an about 90° rotation with changes in the orientation of M1–M3 helices and domain N rotates

by about 20 partially closing the gap between the N and P domains. FITC-labeled Ca^{2+}-ATPase can be crystallized by mono- or decavanadate (Csermely *et al.*, 1985a; 1985b; Varga *et al.*, 1985). Therefore, the vanadate site required for crystallization remains unaffected by the reaction of Lys515 with FITC (Csermely *et al.*, 1885a), that reduces the affinity of ATP-binding by orders of magnitude (Pick, 1981). However, FITC blocks some decavanadate sites that are not required for crystallization (Csermely *et al.*, 1985a).

The large cytoplasmic loop (residues 329–740) that contains the P and N domains was expressed in *E. coli* (Moutin *et al.*, 1994; 1998). It folds spontaneously into a native-like structure and binds TNP-ATP (K_D = 1.6–1.9 μM) in competition with ATP at a single site. K_D for ATP was 200 μM. The expressed protein can be labeled by FITC on Lys515, and it is cleaved by trypsin at the T1 site (Arg505). However, the specific labeling of Lys492 by TNP-ATP and the crosslinking of Lys492 and Arg678 by glutaraldehyde were lost (Moutin *et al.*, 1998).

The A domain (previously called β sheet domain) is a small isolated cytoplasmic segment of 110 residues (residues 131–238) located between the M2 and M3 transmembrane helices (Fig. 3); it interacts with the 40 residue-long N-terminal segment that forms two helices. The A domain structure is modulated by Ca^{2+}. The cleavage of Ca^{2+}-ATPase by trypsin at the T2 site (Arg198) is inhibited in a Ca^{2+}-free medium either by vanadate or by phosphorylation with inorganic phosphate (Dux & Martonosi, 1983b; Immamura *et al.*, 1984; Andersen & Jorgensen, 1985; Dux *et al.*, 1985a). Ca^{2+} also affected the cleavage of Ca^{2+}-ATPase by proteinase K at Lys120 and Asp243 and by V8 protease (Yuul *et al.*, 1995; Danko *et al.*, 2001a; 2001b).

The high resolution structure of the transmembrane domain confirmed the existence of 10 transmembrane helices, but the folding pattern of these helices is different from earlier predictions (Toyoshima *et al.*, 2000) (Fig. 3). Helix M5 is very long (about 60 Å); it extends from the lumenal surface to the center of the P domain and together with helix M4 forms the connections to the large cytoplasmic loop that contains the P and N domains (Fig. 3). Helices M2 and M3 also extend beyond the membrane and serve as anchorage site for the small cytoplasmic loop that contains the A domain. Helices M4, M6 and M10 are unwound near the middle of the membrane (Toyoshima *et al.*, 2000; Soulie *et al.*, 1999). Lumenal loops are short except the one between M7 and M8 (loop L78) that contains 35 residues. A possible site for thapsigargin binding was located at Phe256 near the cytoplasmic membrane interface of M3 (Yu *et al.*, 1998).

Two high density peaks detected near the middle of the bilayer surrounded by helices M4, M5, M6 and M8 were identified as two bound calcium ions (Toyoshima *et al.*, 2000) (Fig. 3). The two Ca^{2+} sites (I and II) are 5.7 Å apart at the same level of the bilayer, within 2.2–2.6 Å from six coordinating oxygen atoms. Site I is between M5 and M6 with contributions from side chain oxygens of Asn768 (M5), Glu771 (M5), Thr799 (M6), Asp800 (M6), and Glu908 (M8). There is a water molecule adjacent to the bound Ca^{2+} in site I. Site II is formed largely on M4 with contributions by carbonyl oxygens of Val304 (M4), Ala305 (M4) and Ile307 (M4) and side chain oxygens of Glu309 (M4), Asn796 (M6) and Asp800 (M6). Asp800 is coordinated to both calcium ions. The two sites are stabilized by hydrogen bond networks that together with Asp800 account for the cooperativity of Ca^{2+} binding.

Calcium ions may enter the Ca^{2+} sites through a cavity between M2, M4, and M6 and exit to the lumen between M3, M4, and M5 (Toyoshima *et al.*, 2000). Mutagenesis data support the role of the N-terminal region of the M3 helix in the control of the access to the Ca^{2+} binding sites (Andersen *et al.*, 2001). A less likely alternative is an entry pathway near M1 lined by Glu58, Glu109 and Glu55 that leads to Ca^{2+} site II (Lee & East, 2001).

The route from the Ca^{2+} sites to the SR lumen probably opens as a result of a conformational change during Ca^{2+} transport. The conditions governing the kinetics of the entry and exit process are still not fully settled (Forge *et al.*, 1995; Canet *et al.*, 1996; Mintz & Guillain, 1997).

The absence of lanthanide binding in the membrane domain (Toyoshima *et al.*, 2000) is consistent with earlier observations that most of the lanthanides are bound to Ca^{2+}-ATPase in the stalk region and near the phospholipid head groups, outside the membrane domain (Asturias & Blasie, 1991; DeLong & Blasie, 1993; Asturias *et al.*, 1994a).

In the classical interpretation of Ca^{2+} transport the two high affinity Ca^{2+} sites of the phosphorylated Ca^{2+}-ATPase are converted into low affinity sites before Ca^{2+} is released into the lumen of SR (Mintz & Guillain, 1997). Some recent results (Meszaros & Bak, 1992; 1993; Jencks *et al.*, 1993; Myung & Jencks, 1994; 1995; Lee, 2002) were interpreted, however, in terms of four Ca^{2+} binding sites per ATPase, assuming that the two high affinity Ca^{2+} binding sites coexist with two low affinity Ca^{2+} sites on each ATPase molecule. In the multilamellar Ca^{2+}-ATPase crystals preserved in 10 mM $CaCl_2$ at pH 6.1, all Ca^{2+} sites are expected to be saturated. While low affinity Ca^{2+} sites may be difficult to resolve, the finding of only two well-defined Ca^{2+} binding sites (Toyoshima *et al.*, 2000) tends to reinforce the classical interpretation of two Ca^{2+} sites with alternating affinity.

Earlier chemical modification, mutagenesis, fluorescence, lamellar X-ray diffraction, and electron crystallography studies suggested that major conformational changes accompany ATP hydrolysis and Ca^{2+} transport (Andersen, 1995; Moller *et al.*, 1996; Mintz & Guillain, 1997; McIntosh, 1998; Lee & East, 2001; Lee, 2002). The scope and structural basis of these changes is becoming clearer with the high resolution structure (MacLennan & Green, 2000; McIntosh, 2000; Toyoshima *et al.*, 2000; Green & MacLennan, 2002; Lancaster, 2002; Toyoshima & Nomura, 2002). The nucleotide-binding pocket is about 80 Å away from the bound calcium ions and the site of phosphorylation, Asp351 is more than 25 Å away from the bound nucleotide (Toyoshima *et al.*, 2000). The two residues cross-linked by glutaraldehyde, Lys492 and Arg678 (McIntosh *et al.*, 1992), are also separated by more than 25 Å (Toyoshima *et al.*, 2000). These data suggest that domains P and N are brought close together during ATP hydrolysis or in the occluded state stabilized by CrATP. Ca^{2+} binding affects the availability of Lys492 for reaction with adenosine triphosphopyridoxal (Yamamoto, 1989), facilitates the cross-linking of Asp351 to Lys684 by ATP imidazolidate (Gutowski-Eckel *et al.*, 1993), changes the reactivities of the enzyme with ATP and P_i (Mintz & Guillain, 1997) and alters the sensitivity of cleavage sites to trypsin (Dux & Martonosi, 1983b; Imamura *et al.*, 1984; Andersen & Jorgensen, 1985; Dux *et al.*, 1985b), proteinase K (Yuul *et al.*, 1995), V8 protease (Danko *et al.*, 2001a; 2001b) and vanadate (Vegh *et al.*, 1990; Molnar *et al.*, 1991; Hua *et al.*, 2000). These changes are presumably brought about by a Ca^{2+}-induced reorientation of the transmembrane helices that are transmitted to the cytoplasmic domains. The loop L67 between helices M6 and M7 probably plays an important role in the coordination of these movements (Falson *et al.*, 1997; Menguy *et al.*, 1998; Zhang *et al.*, 2001).

There is extensive homology between the SERCA type Ca^{2+}-ATPase and the Na^+,K^+-ATPase, that extends through all ten transmembrane domains (Hebert *et al.*, 2001; Rice *et al.*, 2001; Sweadner & Donnet, 2001). These structural similarities provide the basis for the observed similarities between the two enzymes in the mechanism of ion transport (Apell & Karlish, 2001; Jorgensen & Pedersen, 2001; Glynn, 2002). Homology modeling of the Na^+- and K^+-binding sites of the Na^+,K^+-ATPase was carried out (Ogawa & Toyoshima, 2002) based on the structures of Ca^{2+}- bound (Toyoshima *et al.*, 2000) and Ca^{2+}

-free (Toyoshima & Nomura, 2002) forms of the Ca^{2+}-ATPase. The model identified three Na^{+}- and two K^{+}-binding sites, with reciprocal binding of the two ions and explained the kinetic effects of several site specific mutations (Ogawa & Toyoshima, 2002).

Crystal structure of the CA^{2+}-ATPase in a Ca^{2+}-free state at 3.1 Å resolution

The affinity-purified Ca^{2+}-ATPase was complexed with thapsigargin and crystallized by dialysis against a buffer containing 2.75 M glycerol, 4% polyethyleneglycol (PEG 400), 3 mM $MgCl_2$, 2.3 mM sodium azide, 2 μg/ml butylhydroxytoluene, 0.2 mM dithiothreitol, 0.1 mM EGTA, and 20 mM Mes buffer, pH 6.1 (Green & MacLennan, 2002; Toyoshima & Nomura, 2002; Lancaster, 2002). Thapsigargin is an inhibitor of Ca^{2+}-ATPase that is assumed to stabilize the enzyme in a Ca^{2+}-free E_2TG state that may be analogous to the kinetically defined E_2 form (Stokes & Lacapere, 1994; Sagara *et al.*, 1992). Two types of crystals of different symmetry (P21 and P41) were obtained but only the P41 was analyzed in detail.

The three cytoplasmic domains (A, P, and N) that were widely separated in the open structure of the Ca^{2+}-induced crystals (Toyoshima *et al.*, 2000; Ogawa *et al.*, 1998) are closely associated in the Ca^{2+}-free E_2TG state (Toyoshima & Nomura, 2002; Green & MacLennan, 2002; Lancaster, 2002; Toyoshima *et al.*, 2003); they form a compact cytoplasmic domain in which the nucleotide-binding site and the phosphorylation site move close to each other (Fig. 4). This is achieved by the horizontal rotation of the A domain by 110ş, causing the inclination of the N domain by nearly 90 with respect to the membrane and by 50 with respect to the P domain. The P domain is inclined by about 30 with respect to the membrane, linked to the tilting of transmembrane helices. The closed configuration of the Ca^{2+}-free state is stabilized by interactions at the A-N and A-P interfaces without much change in the internal structure of the P and N domains relative to the Ca^{2+}-bound state.

The dissociation of Ca^{2+} from the high affinity sites occurs with rearrangement of transmembrane helices M1-M6 (Toyoshima & Nomura, 2002). Helices M1 and M2 move up toward the cytoplasm, while M3 and M4 move down toward the lumen by about 5 Å. The inclination of the P domain associated with the bending of M5 causes movements of M3–M6 with decrease in the affinity of Ca^{2+} binding and the release of Ca^{2+} from the binding sites (Toyoshima & Nomura, 2002). The access pathways to the Ca^{2+} binding sites remain ill-defined, but Glu309 is likely to play a role in the entry, while the lumenal loops L34 and L78 in the exit of Ca^{2+}. The Ca^{2+}-binding sites are not freely accessible from the lumen in the E_2TG state.

The binding site of thapsigargin is located in a cavity between helices M3, M5, and M7. Thapsigargin binding may stabilize the Ca^{2+}-free E_2TG state by decreasing the mobility of transmembrane helices (Toyoshima & Nomura, 2002). A similar role may be played by Ca^{2+} in stabilizing the detergent-solubilized Ca^{2+}-ATPase in the multilamellar crystals (Pikula *et al.*, 1988; Taylor *et al.*, 1988b).

The transition between the open structure of Ca^{2+}-ATPase in the Ca^{2+}-induced multilamellar crystals (Toyoshima *et al.*, 2000; Ogawa *et al.*, 1998) and the closed structure in the E_2vanadate (Toyoshima *et al.*, 1993; Zhang *et al.*, 1998) or E_2TG state (Toyoshima & Nomura, 2002) cannot be confidently assigned to the structural transition between the kinetically defined E_1Ca_2 and E_2 states of the Ca^{2+}-ATPase for several reasons.

The E_1Ca_2 state is stabilized at micromolar Ca^{2+} concentrations, that do not induce the formation of multilamellar Ca^{2+}-ATPase crystals. The stabilization of E_1Ca_2 state is due to Ca^{2+} binding to the two high affinity Ca^{2+}-binding sites of the Ca^{2+}-ATPase (MacLennan *et al.*, 1997; Mintz & Guillain, 1997; MacLennan & Green, 2000) that induces the formation of

tubular P1 type crystals (Dux *et al.*, 1985b; Ting-Beall *et al.*, 1987).

The Ca^{2+}-induced multilamellar Ca^{2+}-ATPase crystals are formed only at 10–20 mM Ca^{2+} concentrations, presumably due to Ca^{2+} binding to low affinity Ca^{2+} binding sites, and are distinct from the P1 type tubular crystals formed at micromolar Ca^{2+} (Dux *et al.*, 1985b; Ting-Beall *et al.*, 1987).

Raising the Ca^{2+} concentration from 0.1 mM to 10–20 mM causes the appearance of an infrared peak at 1650 cm^{-1} (Arrondo *et al.*, 1987). This peak is absent in the E_1Ca_2 state stabilized by 0.1 mM $CaCl_2$, but present in the E_2vanadate state stabilized by vanadate in Ca^{2+}-free solutions (Arrondo *et al.*, 1987). Differences between infrared spectra obtained at low and high Ca^{2+} concentration were also seen in phospholipid extracts of SR at 1741 cm^{-1} (Arrondo *et al.*, 1987). The changes in the infrared spectra induced by 10–20 mM Ca^{2+} suggest structural changes both in the Ca^{2+}-ATPase and in the lipid phase that are not characteristic of the kinetically defined E_1Ca_2 state. The possibility of Ca^{2+} effects on minor SR protein components are difficult to exclude.

These observations imply that the high (10–20 mM) Ca^{2+} concentrations required to

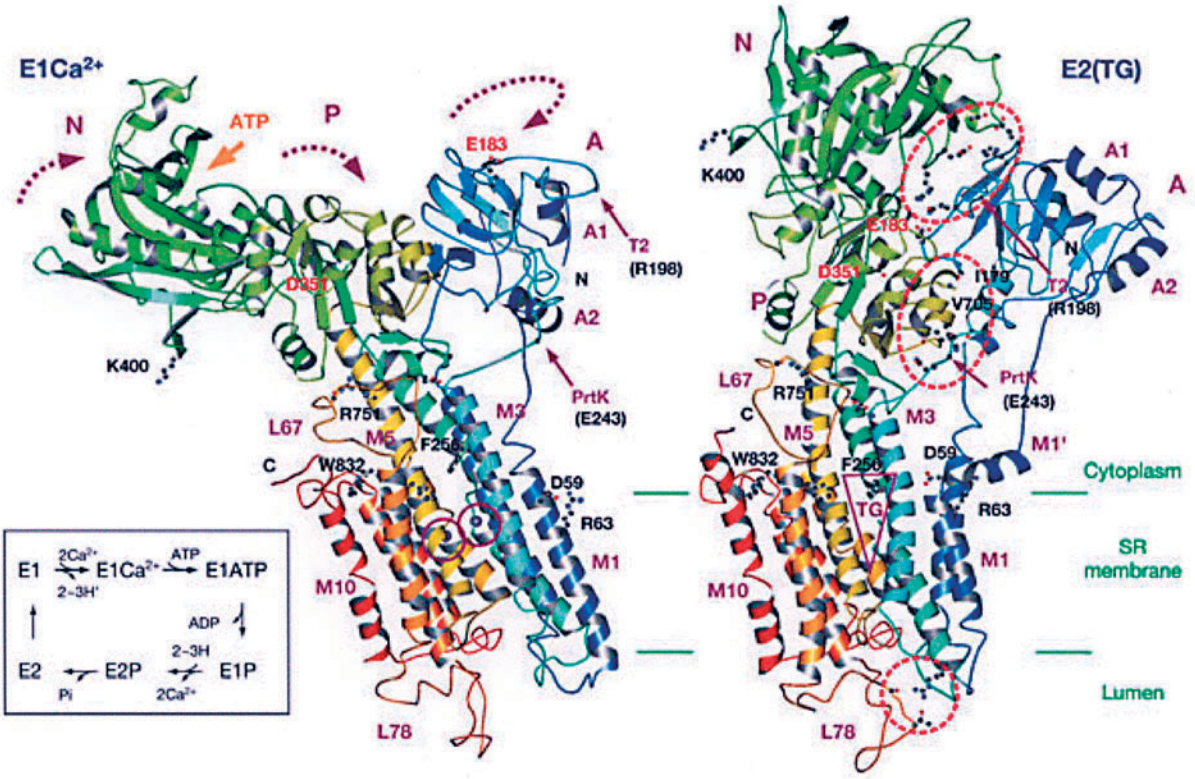

Figure 4. Ribbon representation of SR Ca^{2+}-ATPase in the Ca^{2+}-bound form (E_1Ca^{2+}) and that of the E_2(TG) form in the absence of Ca^{2+} but in the presence of thapsigargin (TG).

Inset, a simplified reaction scheme showing only the forward reactions. Colours change gradually from the amino terminus (blue) to the carboxy terminus (red). Two purple spheres (circled) in E_1Ca^{2+} represent bound Ca^{2+}. Red circles in E_2(TG) indicate extra hydrogen bonds. Large arrows in E_1Ca^{2+} indicate the direction of movement of the cytoplasmic domains during the change from E_1Ca^{2+} to E_2(TG). PtrK, proteinase-K digestion site (around Glu243); T2, trypsin digestion site at Arg198; ATP, binding pocket for the adenosine moiety of ATP. Principal residues are marked: Glu183 (A domain), Phe256 (thapsigargin-binding site), Asp351 (P domain, phosphorylation site), Lys400 (N domain, phospholamban-binding site) and Arg751 (linking M5 and the loop (L67) connecting M6 and M7). Prepared with MOLSCRIPT. Modified from Toyoshima & Nomura (2002). Printed with permission from Nature Publishing Group.

produce the multilamellar Ca^{2+}-ATPase crystals may induce secondary effects on the structure of Ca^{2+}-ATPase, making the conformational assignment to the kinetically defined E_1Ca_2 state (Toyoshima *et al.*, 2000; Toyoshima & Nomura, 2002) arbitrary. The P1 type Ca^{2+}-ATPase crystals induced by 0.1 mM Ca^{2+} in sarcoplasmic reticulum vesicles are more plausible representatives of the kinetically defined E_1Ca_2 state (Dux *et al.*, 1985b; Ting-Beall *et al.*, 1987). Unfortunately no high resolution structure is available for this crystal form. Further studies are required to establish the relevance of the multilamellar Ca^{2+}-induced crystals to the kinetically defined E_1Ca_2 state.

LAMELLAR X-RAY AND NEUTRON DIFFRACTION ANALYSIS OF THE PROFILE STRUCTURES OF Ca^{2+}-ATPase IN SARCOPLASMIC RETICULUM MULTILAYERS

Blasie and his colleagues have determined the separate profile structures of the lipid bilayer and of the Ca^{2+} transport ATPase molecule within the sarcoplasmic reticulum membrane to 11 Å resolution by a combination of X-ray and neutron diffraction techniques (Blasie *et al.*, 1985; Herbette *et al.*, 1985).

In oriented, partially dehydrated multilayers, under conditions suitable for X-ray diffraction studies, the SR vesicles retain much of their ATP-energized Ca^{2+} transport activity. The Ca^{2+} transport can by initiated by flash-photolysis of P^3-1(2-nitro)phenylethyladenosine-5′-triphosphate (caged ATP). The flash photolysis of caged ATP rapidly releases ATP and effectively synchronizes the Ca^{2+} transport cycle of the ensemble of Ca^{2+}-ATPase molecules (Blasie *et al.*, 1985). Time resolved changes in the profile structure of the sarcoplasmic reticulum during Ca^{2+} transport imply that associated with enzyme phosphorylation, about 8% of the mass of the Ca^{2+}-ATPase is redistributed from the extravesicular surface to the membrane bilayer region and to the intravesicular surface within 200–500 msec after the flash- photolysis of caged ATP (Blasie *et al.*, 1985; 1990). During the next five seconds there was no further change in the profile structure, although the Ca^{2+}-ATPase completed several cycles of Ca^{2+} transport. This may be explained by assuming that the $E_1 \sim P$ form of the enzyme is the dominant intermediate during the steady state. La^{3+} and Tb^{3+} also activate the phosphorylation of Ca^{2+}-ATPase (Asturias *et al.*, 1994b) and the Tb^{3+} induced phosphoenzyme formation was accompanied by decrease in electron density in the outer phospholipid monolayer and an increase in the inner phospholipid monolayer. These changes are qualitatively similar to those observed in the presence of Ca^{2+} (Herbette *et al.*, 1985; Blasie *et al.*, 1990) but smaller in magnitude due perhaps to the lower steady state concentrations of $E \sim P$ found in the presence of Tb^{3+} (Asturias *et al.*, 1994b).

In contrast to the effects associated with enzyme phosphorylation, low temperature and low Mg^{2+} concentration cause the redistribution of Ca^{2+}-ATPase mass from the lipid hydrocarbon region into the cytoplasm (Pascolini & Blasie, 1988; Pascolini *et al.*, 1988; Asturias *et al.*, 1989; 1990). These effects of temperature and Mg^{2+} concentration on the structure of the lipid phase and on the transmembrane disposition of Ca^{2+}-ATPase are manifested in slower rate of E_1P formation and longer lifetime of E_1P at near 0°C temperature and at low Mg^{2+} concentration (Pascolini & Blasie, 1988; Pascolini *et al.*, 1988; Asturias *et al.*, 1989; 1990).

Photolysis of the calcium chelator DM nitrophen can be used to rapidly release Ca^{2+} in SR multilayers (DeLong & Blasie, 1993). Ca^{2+}-binding to the SR in the absence of ATP caused increased electron density in three regions of the membrane profile, corresponding to the intravesicular membrane surface, the center of the bilayer and the junction of the stalk and headpiece regions of the cytoplasmic

domain of the Ca^{2+}-ATPase (DeLong & Blasie, 1993). The Ca^{2+}-binding site in the center of the bilayer corresponds to the location identified by X-ray analysis of multilamellar Ca^{2+}-ATPase crystals (Toyoshima *et al.*, 2000). The Ca^{2+}-binding sites on the inner surface and in the stalk region may be related to negatively charged regions of the Ca^{2+}-ATPase near the entrance and exit of the Ca^{2+} channel. Ca^{2+}-binding to these sites is associated with a decrease in electron density in the adjacent regions, suggesting conformational changes in the Ca^{2+}-ATPase associated with Ca^{2+}-binding (DeLong & Blasie, 1993). La^{3+} and Tb^{3+} are bound with high affinity to the stalk portion of the cytoplasmic domain about 12 Å from the phospholipid head group region of cytoplasmic membrane surface. This site accounts for about 80% of the bound lanthanides. The remainder is bound with lower affinity near the phospholipid head groups on the cytoplasmic and lumenal membrane surface (Asturias & Blasie, 1991; Asturias *et al.*, 1994a; Blasie *et al.*, 1992). Tb^{3+}, in contrast to La^{3+}, also binds to the site in the center of the bilayer presumably in competition with Ca^{2+} (Asturias *et al.*, 1994a; Blasie *et al.*, 1992). Phosphorylation of Ca^{2+}-ATPase induced by Tb^{3+} causes the movement of metal density toward the intravesicular surface presumably due to changes in the affinity of the various metal binding sites (Asturias *et al.*, 1994a).

TARGETING AND INSERTION OF THE Ca^{2+}-ATPase TO THE SARCOPLASMIC RETICULUM

The SR Ca^{2+}-ATPases are synthesized on membrane-bound polysomes and cotranslationally inserted into the sarcoplasmic reticulum membrane (Martonosi, 2000). The role of various Ca^{2+}-ATPase domains in targeting and insertion was analyzed by *in vitro* transcription-translation scanning (Bayle *et al.*, 1995), and by constructing chimeras of the SERCA Ca^{2+}-ATPase with the plasma membrane Ca^{2+}-ATPase (PMCA) (Foletti *et al.*, 1995; Newton *et al.*, 2003), that possess distinct targeting information. Transmembrane domains M1, M2, M3, M4, M7 and M9 acted both as signal anchor and stop-transfer sequences while domains M5, M8 and M10 acted only as stop-transfer sequences (Bayle *et al.*, 1995; Newton *et al.*, 2003). Transmembrane domain M6 did not insert cotranslationally into the membrane. The extended C-terminal region of SERCA2b had both signal anchor and stop-transfer capacity, consistent with serving as an eleven transmembrane domain; this would place the C terminus of SERCA2b on the lumenal side, while SERCA1 and 2a have both ends on the cytoplasmic side. The absence of signal anchor sequence in M5 suggests that it does not insert independently, while M7 and M8 are probably inserted as a pair. There is no indication that the Ca^{2+}-ATPase forms stable interaction with immunoglobulin binding protein (BiP) or other chaperons (Karin & Settle, 1992). Replacing the N-terminus of PMCA with the 85 N-terminal residues of SERCA was sufficient to direct retention of the plasma membrane Ca^{2+}-ATPase in the ER (Foletti *et al.*, 1995). Since truncated PMCA lacking the N-terminal 204 amino-acid residues was still expressed in the plasma membrane, the SERCA N-terminus overrides the tendency of PMCA for plasma membrane localization. These observations indicate the presence of an endoplasmic retention signal in the N-terminal segment of SERCA Ca^{2+}-ATPase. The Ca^{2+}-ATPase does not contain the Lys-Asp-Glu-Leu/His-Asp-Glu-Leu or the Lys-Lys-XX and Lys-X-Lys-X-Lys-X sequences that direct other proteins to the endoplasmic reticulum.

REFERENCES

Andersen JP, Jorgensen PL. (1985)
Conformational states of sarcoplasmic reticulum Ca^{2+}-ATPase as studied by proteolytic cleavage. *J Membr Biol.*; **88**: 187–98.

Andersen JP, Sorensen TL, Povlsen K, Vilsen B. (2001) Importance of transmembrane segment M3 of the sarcoplasmic reticulum Ca^{2+}-ATPase for control of the gateway to the Ca^{2+} sites. *J Biol Chem.*; **276**: 23312–21.

Andersen JP. (1995) Dissection of the functional domains of the sarcoplasmic reticulum Ca^{2+} ATPase by site directed mutagenesis. *Biosci Rep.*; **15**: 243–61.

Andersen JP. (1989) Monomer oligomer equilibrium of sarcoplasmic reticulum Ca^{2+}-ATPase and the role of subunit interaction in the Ca^{2+} pump mechanism. *Biochim Biophys Acta.*; **988**: 47–72.

Apell H-J, Karlish SJ. (2001) Functional properties of Na-K ATPase and their structural implications as detected by biophysical techniques. *J Membr Biol.*; **180**: 1–9.

Aravind L, Galperin MY, Koonin EV. (1998) The catalytic domain of the P-type ATPase has the haloacid dehalogenase fold. *Trends Biochem Sci.*; **23**: 127–9.

Arrondo JLR, Mantsch HH, Mullner N, Pikula S, Martonosi A. (1987) Infrared spectroscopic characterization of the structural changes connected with the E1→E2 transition in the Ca^{2+}-ATPase of sarcoplasmic reticulum. *J Biol Chem.*; **262**: 9037–43.

Asturias FJ, Blasie JK. (1989) Effect of Mg^{2+} concentration on Ca^{2+} uptake kinetics and structure of the sarcoplasmic reticulum membrane. *Biophys J.*; **55**: 739–53.

Asturias FJ, Blasie JK. (1991) Location of high affinity metal binding sites in the profile structure of the Ca^{2+}-ATPase in the sarcoplasmic reticulum by resonance X-ray diffraction. *Biophys J.*; **59**: 488–502.

Asturias FJ, Fischetti RJ, Blasie JK. (1994a) Changes in the relative occupancy of metal binding sites in the profile structure of the sarcoplasmic reticulum membrane induced by phosphorylation of the Ca^{2+}-ATPase enzyme in the presence of terbium: a time-resolved X-ray diffraction study. *Biophys J.*; **66**: 1665–77.

Asturias FJ, Fischetti RF, Blasie JK. (1994b) Changes in the profile structure of the sarcoplasmic reticulum membrane induced by phosphorylation of the Ca^{2+}-ATPase enzyme in the presence of terbium: a time-resolved X-ray diffraction study. *Biophys J.*; **66**: 1653–64.

Asturias FJ, Pascolini D, Blasie JK. (1990) Evidence that lipid lateral phase separation induces functionally significant structural changes in the Ca^{2+} ATPase of sarcoplasmic reticulum. *Biophys J.*; **58**: 205–17.

Baskin RJ, Deamer DW. (1969) Comparative ultrastructure and calcium transport in heart and skeletal muscle microsomes. *J Cell Biol.*; **43**: 610–5.

Bayle D, Weeks D, Sachs G. (1995) The membrane topology of the rat sarcoplasmic and endoplasmic reticulum calcium ATPases by in vitro translation scanning. *J Biol Chem.*; **270**: 25678–84.

Beeler TJ, Dux L, Martonosi AN. (1984) Effect of Na_3VO_4 and membrane potential on the structure of sarcoplasmic reticulum membrane. *J Membr Biol.*; **78**: 73–9.

Bigelow DJ, Inesi G. (1992) Contributions of chemical derivatization and spectroscopic studies to the characterization of the Ca^{2+} transport ATPase of sarcoplasmic reticulum. *Biochim Biophys Acta.*; **1113**: 323–38.

Blasie JK, Asturias FJ, DeLong LJ. (1992) Time-resolved X-ray diffraction studies on the mechanism of active Ca^{2+} transport by the sarcoplasmic reticulum Ca^{2+}-ATPase. *Ann NY Acad Sci.*; **671**: 11–8.

Blasie JK, Herbette L, Pachence J. (1985a) Biological membrane structure as seen by X-ray and neutron diffraction techniques. *J Membr Biol.*; **86**: 1–7.

Blasie JK, Herbette LG, Pascolini D, Skita V, Pierce DH, Scarpa A. (1985b) Time resolved X-ray diffraction studies of the sarcoplasmic reticulum membrane during active transport. *Biophys J.*; **48**: 9–18.

Blasie JK, Pascolini D, Asturias F, Herbette LG, Pierce D, Scarpa A. (1990) Large-scale structural changes in the sarcoplasmic reticulum appear essential for calcium transport. *Biophys J.*; **58**: 687–93.

Boland R, Martonosi A, Tillack TW. (1974) Developmental changes in the composition and function of sarcoplasmic reticulum. *J Biol Chem.*; **249**: 612–23.

Brandl CJ, Green NM, Korczak B, MacLennan DH. (1986) Two Ca^{2+}-ATPase genes: Homologies and mechanistic implications of deduced amino acid sequences. *Cell.*; **44**: 597–607.

Brandl CJ, deLeon S, Martin S, MacLennan DH. (1987) Adult forms of the Ca^{2+}-ATPase of sarcoplasmic reticulum. Expression in developing skeletal muscle. *J Biol Chem.*; **262**: 3768–74.

Burk SE, Lytton J, MacLennan DH, Shull GE. (1989) cDNA cloning, functional expression and mRNA tissue distribution of a third organellar Ca^{2+} pump. *J Biol Chem.*; **264**: 18561–8.

Canet D, Forge V, Guillain F, Mintz E. (1996) Ca^{2+} translocation across sarcoplasmic reticulum ATPase randomizes the two transported ions. *J Biol Chem.*; **271**: 20566–72.

Castellani L, Hardwicke PMD, Vibert P. (1985) Dimer ribbons in the three-dimensional structure of sarcoplasmic reticulum. *J Mol Biol.*; **185**: 579–94.

Caswell AH, Brandt NR, Brunschwig J-P, Purkerson S. (1988) Isolation of transverse tubule membranes from skeletal muscle: Ion transport activity, reformation of triad junctions and isolation of junctional spanning protein of triads. *Methods Enzymol.*; **157**: 68–84.

Cheong G-W, Young HS, Ogawa H, Toyoshima C, Stokes DL. (1996) Lamellar stacking in three-dimensional crystals of Ca^{2+}-ATPase from sarcoplasmic reticulum. *Biophys J.*; **70**: 1689–99.

Chu A, Dixon MC, Saito A, Seiler S, Fleischer S. (1988) Isolation of sarcoplasmic reticulum fractions referable to longitudinal tubules and junctional terminal cisternae from rabbit skeletal muscle. *Methods Enzymol.*; **157**: 36–46.

Coan C, Scales DJ, Murphy AJ. (1986) Oligovanadate binding to sarcoplasmic reticulum. Evidence for substrate analogue behaviour. *J Biol Chem.*; **261**: 10394–403.

Coan C, Ji JY, Amaral JA. (1994) Ca^{2+} binding to occluded sites in the CrATP-ATPase complex of sarcoplasmic reticulum: evidence for two independent high affinity sites. *Biochemistry.*; **33**: 3722–31.

Costello B, Chadwick C, Fleischer S. (1988) Isolation of the junctional face membrane of sarcoplasmic reticulum. *Methods Enzymol.*; **157**: 46–50.

Csermely P, Katopis C, Wallace BA. (1987) The $E_1 \rightarrow E_2$ transition of Ca^{2+}-ATPase in sarcoplasmic reticulum occurs without major changes in secondary structure. *Biochem J.*; **241**: 663–9.

Csermely P, Martonosi A, Levy GC, Ejchart AJ. (1985a) ^{51}V-nmr analysis of the binding of vanadium (V) oligoanions to sarcoplasmic reticulum. *Biochem J.*; **230**: 807–15.

Csermely P, Varga S, Martonosi A. (1985b) Competition between decavanadate and fluorescein isothiocyanate on the Ca^{2+}-ATPase of sarcoplasmic reticulum. *Eur J Biochem.*; **150**: 455–60.

Danko S, Daiho T, Yamasaki K, Kamidochi M, Suzuki H, Toyoshima C. (2001a) ADP insensitive phosphoenzyme intermediate of sarcoplasmic reticulum Ca^{2+}-ATPase has a compact conformation resistant to proteinase K, V8 protease and trypsin. *FEBS Lett.*; **489**: 277–82.

Danko S, Yamasaki K, Daiho T, Suzuki H, Toyoshima C. (2001b) Organizationn of cytoplasmic domains of sarcoplasmic reticulum Ca^{2+}-ATPase in E_1P and E_1ATP states: a limited proteolysis study. *FEBS Lett.*; **505**: 129–35.

DeLong LJ, Blasie JK. (1993) Effect of Ca^{2+} binding on the profile structure of the sarcoplasmic reticulum membrane using time resolved X-ray diffraction. *Biophys J.*; **64**: 1750–9.

Dode L, Wuytack F, Kools PF, Baba-Aissa F, Raeymaekers L, Brike F, van de Ven WJ, Casteels R, Brik F. (1996) cDNA cloning, expression and chromosomal localizationn of

the human sarco/endoplasmic reticulum Ca^{2+}-ATPase 3 gene. *Biochem J.*; **318**: 689–99.

Dux L, Martonosi A. (1983a) Two-dimensional arrays of proteins in sarcoplasmic reticulum and purified Ca^{2+}-ATPase vesicles treated with vanadate. *J Biol Chem.*; **258**: 2599–603.

Dux L, Martonosi A. (1983b) Ca^{2+}-ATPase membrane crystals in sarcoplasmic reticulum. The effect of trypsin digestion. *J Biol Chem.*; **258**: 10111–5.

Dux L, Martonosi A. (1983c) The regulation of ATPase-ATPase interactions in sarcoplasmic reticulum membranes. I. The effects of Ca^{2+}, ATP and inorganic phosphate. *J Biol Chem.*; **258**: 11896–902.

Dux L, Martonosi A. (1983d) The regulation of ATPase-ATPase interactions in sarcoplasmic reticulum membranes II. The influence of membrane potential. *J Biol Chem.*; **258**: 11903–7.

Dux L, Martonosi A. (1984) Membrane crystals of Ca^{2+}-ATPase in sarcoplasmic reticulum of fast and slow skeletal and cardiac muscles. *Eur J Biochem.*; **141**: 43–9.

Dux L, Papp S, Martonosi A. (1985a) Conformational responses of the tryptic cleavage products of the Ca^{2+}-ATPase of sarcoplasmic reticulum. *J Biol Chem.*; **260**: 13454–8.

Dux L, Pikula S, Mullner N, Martonosi A. (1987) Crystallization of Ca^{2+}-ATPase in detergent-solubilized sarcoplasmic reticulum. *J Biol Chem.*; **262**: 6439–42.

Dux L, Taylor KA, Ting-Beall HP, Martonosi A. (1985b) Crystallization of the Ca^{2+}-ATPase of sarcoplasmic reticulum by calcium and lanthanide ions. *J Biol Chem.*; **260**: 11730–43.

Ebashi S. (1961) Calcium binding activity of vesicular relaxing factor. *J Biochem.*; **50**: 236–44.

Ebashi S, Lipmann F. (1962) Adenosine triphosphate-linked concentration of calcium ions in a particulate fraction of rabbit muscle. *J Cell Biol.*; **14**: 389–400.

Falson P, Menguy T, Corre F, Bouneau L, de Gracia AG, Soulie S, Centeno F, Moller JV, Champeil P, le Maire M. (1997) The cytoplasmic loop between putative transmembrane segments 6 and 7 in sarcoplasmic reticulum Ca^{2+}-ATPase binds Ca^{2+} and is functionally important. *J Biol Chem.*; **272**: 17258–62.

Ferguson DG, Franzini-Armstrong C, Castellani L, Hardwicke PM, Kenney LJ. (1985) Ordered arrays of Ca^{2+}-ATPase on the cytoplasmic surface of isolated sarcoplasmic reticulum. *Biophys J.*; **48**: 597–605.

Foletti D, Guerini D, Carafoli E. (1995) Subcellular targeting of the endoplasmic reticulum and plasma membrane calcium pumps: a study using recombinant chimeras. *FASEB J.*; **9**: 670–80.

Forge V, Mintz E, Canet D, Guillain F. (1995) Lumenal Ca^{2+} dissociation from the phosphorylated Ca^{2+}-ATPase of the sarcoplasmic reticulum is sequential. *J Biol Chem.*; **270**: 18271–6.

Franzini-Armstrong C, Ferguson DG. (1985) Density and disposition of Ca^{2+} ATPase in sarcoplasmic reticulum membrane as determined by shadowing techniques. *Biophys J.*; **48**: 607–15.

Girardet J-L, Dupont Y, Lacapere JJ. (1989) Evidence of a Ca^{2+}-induced structural change in the ATP-binding site of the sarcoplasmic reticulum Ca^{2+}-ATPase using terbium formycin triphosphate as an analogue of Mg-ATP. *Eur J Biochem.*; **184**: 131–40.

Glynn IM. (2002) A hundred years of sodium pumping. *Annu Rev Physiol.*; **64**: 1–18.

Green NM, MacLennan DH. (2002) Calcium callisthenics. *Nature.*; **418**: 598–99.

Green NM, Stokes DL. (1992) Structural modelling of P-type ion pumps. *Acta Physiol Scand (Suppl.).*; **146 (607)**: 59–68.

Gunteski-Humblin A-M, Greeb J, Shull GE. (1988) A novel Ca^{2+} pump expressed in brain, kidney, and stomach is encoded by an alternative transcript of the slow-twitch muscle sarcoplasmic reticulum Ca-ATPase gene. Identification of cDNAs encoding Ca^{2+} and other cation-transporting ATPases using an

oligonucleotide probe derived from the ATP-binding site. *J Biol Chem.*; **263**: 15032–40.

Gutowski-Eckel Z, Mann K, Bäumert HG. (1993) Identification of a cross-linked double-peptide from the catalytic site of the Ca^{2+}-ATPase of sarcoplasmic reticulum formed by the Ca^{2+} and pH-dependent reaction with ATP γP-imidazolidate. *FEBS Lett.*; **124**: 314–8.

Hasselbach W, Makinose M. (1961) Die calciumpumpe der "Erschlaffungsgrana" des muskels und ihre abhängigkeit von der ATP-spaltung. *Biochem Z.*; **333**: 518–28.

Hasselbach W, Makinose M. (1963) Über den mechanismus des calciumtransportes durch die membranen des sarkoplasmatischen reticulums. *Biochem Z.*; **339**: 94–111.

Hebert H, Purhonen P, Vorum H, Thomsen K, Maunsbach AB. (2001) Three-dimensional structure of renal Na-K-ATPase from cryo-electron microscopy of two-dimensional crystals. *J Mol Biol.*; **314**: 479–94.

Heilbrunn LV, Wiercinsky FJ. (1947) Action of various cations on muscle protoplasm. *J Cell Comp Physiol.*; **19**: 15–32.

Herbette L, DeFoor P, Fleischer S, Pascolini D, Scarpa A, Blasie JK. (1985) The separate profile structures of the functional calcium pump protein and the phospholipid bilayer within isolated sarcoplasmic reticulum membranes determined by X-ray and neutron diffraction. *Biochim Biophys Acta.*; **817**: 103–22.

Highsmith SR, Head MR. (1983) Tb^{3+} binding to Ca^{2+} and Mg^{2+} binding sites on sarcoplasmic reticulum ATPase. *J Biol Chem.*; **258**: 6858–62.

Hua S, Inesi G, Toyoshima C. (2000) Distinct topologies of mono- and decavanadate binding and photooxidative cleavage in the sarcoplasmic reticulum ATPase. *J Biol Chem.*; **275**: 30546–50.

Ikemoto N, Sreter FA, Nakamura A, Gergely J (1968) Tryptic digestion and localization of calcium uptake and ATPase activity in fragments of sarcoplasmic reticulum. *J Ultrastructure Res.*; **23**: 216–32.

Imamura Y, Saito K, Kawakita M. (1984) Conformational change of Ca^{2+},Mg^{2+}-adenosine triphosphatase of sarcoplasmic reticulum upon binding of Ca^{2+} and adenyl-5′-yl-imidodiphosphate as detected by trypsin sensitivity analysis. *J Biochem.*; **95**: 1305–13.

Jencks WP, Yang T, Peisach D, Myung J. (1993) Calcium ATPase of sarcoplasmic reticulum has four binding sites for calcium. *Biochemistry.*; **32**: 7030–4.

Jilka RL, Martonosi AN, Tillack TW. (1975) Effect of the purified (Mg^{2+}+Ca^{2+})-activated ATPase of sarcoplasmic reticulum upon the passive Ca^{2+} permeability and ultrastructure of phospholipid vesicles. *J Biol Chem.*; **250**: 7511–24.

Jona I, Martonosi A. (1986) The effects of membrane potential and lanthanides on the conformation of the Ca^{2+} transport ATPase in sarcoplasmic reticulum. *Biochem J.*; **234**: 363–71.

Jorgensen PL, Pedersen PA. (2001) Structure-function relationships of Na^+, K^+, ATP or Mg^{2+} binding and energy transduction in Na,K-ATPase. *Biochim Biophys Acta.*; **1505**: 57–74.

Karin NJ, Kaprielian Z, Fambrough DM. (1989) Expression of avian Ca^{2+}-ATPase in cultured mouse myogenic cells. *Mol Cell Biol.*; **9**: 1978–86.

Karin NJ, Settle VJ. (1992) The sarcoplasmic reticulum Ca^{2+}-ATPase SERCA1a contains endoplasmic reticulum targeting information. *Biochem Biophys Res Commun.*; **186**: 219–27.

Kawakami K, Noguchi S, Noda M, Takahashi H, Ohta T, Kawamura M, Nojima H, Nagano K, Hirose T, Inayama S, *et al.* (1985) Primary structure of the α-subunit of *Torpedo californica* (Na^++K^+)ATPase deduced from cDNA sequence. *Nature.*; **316**: 733–6.

Korczak B, Zarain-Herzberg A, Brandl CJ, Ingles CJ, Green NM, MacLennan DH. (1988) Structure of the rabbit fast-twitch skeletal muscle Ca^{2+}-ATPase gene. *J Biol Chem.*; **263**: 4813–9.

Kovacs T, Felfoldi F, Papp B, Paszty K, Bredoux R, Enyedi A, Enouf J. (2001) All three splice variants of the human sarco/endoplasmic reticulum Ca^{2+}-ATPase gene are translated to proteins: a study of their co-expression in platelets and lymphoid cells. *Biochem J.*, **358**: 559–68.

Lacapere J-J, Stokes DL, Olofsson A, Rigaud JL. (1998) Two dimensional crystallization of Ca^{2+}-ATPase by detergent removal. *Biophysical J.*; **75**: 1319–29.

Lancaster CRD. (2002) A P-type ion pump at work. *Nat Struct Biol.*; **9**: 643–5.

Lee AG, East M. (2001) What the structure of a calcium pump tells us about its mechanism? *Biochem J.*; **356**: 665–83.

Lee AG. (2002) Ca^{2+}-ATPase structure in the E1 and E2 conformations: mechanism, helix-helix and helix-lipid interactions. *Biochim Biophys Acta.*; **1565**: 246–66.

Lytton J, MacLennan DH. (1988) Molecular cloning of cDNAs from human kidney coding for two alternatively spliced products of the cardiac Ca^{2+}-ATPase gene. *J Biol Chem.*; **263**: 15024–31.

Lytton J, Westlin M, Burk SE, Shull GE, MacLennan DH. (1992) Functional comparisons between isoforms of the sarcoplasmic or endoplasmic reticulum family of calcium pumps. *J Biol Chem.*; **267**: 14483–9.

Lytton J, Zarain-Herzberg A, Periasamy M, MacLennan DH. (1989) Molecular cloning of the mammalian smooth muscle sarco(endo)plasmic reticulum Ca^{2+} ATPase. *J Biol Chem.*; **264**: 7059–65.

MacLennan DH. (2000) Ca^{2+} signalling and muscle disease. *Eur J Biochem.*; **267**: 5291–7.

MacLennan DH, Brandl CJ, Champaneira S, Holland PC, Powers VE, Willard HF. (1987) Fast-twitch and slow-twitch/cardiac Ca^{2+} ATPase genes map to human chromosomes 16 and 12. *Somat Cell Molec Genet.*; **13**: 341–6.

MacLennan DH, Brandl CJ, Korczak B, Green NM. (1985) Amino-acid sequence of a Ca^{2+} + Mg^{2+}-dependent ATPase from rabbit muscle sarcoplasmic reticulum, deduced from its complementary DNA sequence. *Nature.*; **316**: 696–700.

MacLennan DH, Green NM. (2000) Pumping ions. *Nature.*; **405**: 633–4.

MacLennan DH, Rice WJ, Green MN. (1997) The mechanism of Ca^{2+} transport by sarco(endo)plasmic reticulum Ca^{2+} ATPases. *J Biol Chem.*; **272**: 28815–8.

Magyar A, Bakos E, Varadi A. (1995) Structure and tissue-specific expression of the *Drosophila melanogaster* organellar type Ca^{2+}-ATPase gene. *Biochem J.*; **310**: 757–63.

Martonosi A. (1968) Sarcoplasmic reticulum V. The structure of sarcoplasmic reticulum membrane. *Biochim Biophys Acta.*; **150**: 694–704.

Martonosi A. (1992) The Ca^{2+} transport ATPases of sarco(endo)plasmic reticulum and plasma membrane. In *Molecular aspects of transport proteins*. de Pont JJHHM. ed., pp 57–116. Amsterdam, Elsevier.

Martonosi AN. (1995) The structure and interactions of the Ca^{2+}-ATPase. *Biosci Rep.*; **15**: 363–81.

Martonosi A. (2000) *The development of sarcoplasmic reticulum.* Amsterdam, Harwood Academic Publ.

Martonosi A, Pikula S. (2003) The network of calcium regulation in muscle. *Acta Biochim Polon.*; **50**: 1–29.

Martonosi AN, Taylor KA, Pikula S. (1991) The crystallization of the Ca^{2+}-ATPase of sarcoplasmic reticulum. In *Crystallization of membrane proteins*. Michel H. ed., pp 167–82. Boca Raton, CRC Press.

McIntosh DB. (1998) The ATP binding sites of P-type ion transport ATPases: properties, structure, conformations, and mechanism of coupling. *Adv Mol Cell Biol.*; **23A**: 33–99.

McIntosh DB. (1992) Glutaraldehyde cross-links Lys492 and Arg678 at the active site of sarcoplasmic reticulum Ca^{2+}-ATPase. *J Biol Chem.*; **267**: 22328–35.

McIntosh DB. (2000) Portrait of a P-type pump. *Nat Struct* Biol.; **7**: 532–5.

McIntosh DB, Woolley DG. (1994) Catalysis of an ATP analogue untethered and tethered to Lysine 492 of sarcoplasmic reticulum Ca^{2+}-ATPase. *J Biol Chem.*; **269**: 21587–95.

McIntosh DB, Woolley DG, Berman MC. (1992) 2′,3′-*O*(2,4,6-trinitrophenyl)-8-azidoAMP and -ATP photolabel Lys492 at the active site of sarcoplasmic reticulum Ca^{2+} ATPase. *J Biol Chem.*; **267**: 5301–9.

Menguy T, Corre F, Bouneau L, Deschamps S, Moller JV, Champeil P, le Maire M, Falson P. (1998) The cytoplasmic loop located between transmembrane segments 6 and 7 controls activation by Ca^{2+} of sarcoplasmic reticulum Ca^{2+}-ATPase. *J Biol Chem.*; **273**: 20134–43.

Meszaros LG, Bak JZ. (1992) Simultaneous internalization and binding of calcium during the initial phase of calcium uptake by the sarcoplasmic reticulum Ca pump. *Biochemistry.*; **31**: 1195–200.

Meszaros LG, Bak JZ. (1993) Coexistence of high-affinity and low-affinity Ca^{2+}-binding sites of the sarcoplasmic reticulum calcium pump. *Biochemistry.*; **32**: 10085–8.

Michel H. (1990) General and practical aspects of membrane protein crystallization. In *Crystallization of membrane proteins*. Michel H. ed., pp 73–88. Boca Raton, CRC Press.

Mintz E, Guillain F. (1997) Ca^{2+} transport by the sarcoplasmic reticulum ATPase. *Biochim Biophys Acta.*; **1318**: 52–70.

Misra M, Taylor D, Oliver T, Taylor K. (1991) Effect of organic anions on the crystallization of the Ca^{2+}-ATPase of muscle sarcoplasmic reticulum. *Biochim Biophys Acta.*; **1077**: 107–18.

Mitchell RD, Palade P, Saito A, Fleischer S. (1988) Isolation of triads from skeletal muscle. *Methods Enzymol.*; **157**: 51–68.

Moller JV, Juul B, leMaire M. (1996) Structural organization, ion transport and energy transduction of P type ATPases. *Biochim Biophys Acta.*; **1286**: 1–51.

Molnar E, Varga S, Martonosi A. (1991) Differences in the susceptibility of various cation transport ATPases to vanadate catalysed photocleavage. *Biochim Biophys Acta.*; **1068**: 17–26.

Moutin M-J, Cuillel M, Rapin C, Miras R, Anger M, Lompre AM, Dupont Y. (1994) Measurements of ATP binding on the large cytoplasmic loop of the sarcoplasmic reticulum Ca^{2+}-ATPase overexpressed in *Escherichia coli*. *J Biol Chem.*; **269**: 11147–54.

Moutin M-J, Rapin C, Miras R, Vincon M, Dupont Y, McIntosh DB. (1998) Autonomous folding of the recombinant large cytoplasmic loop of sarcoplasmic reticulum Ca^{2+} ATPase probed by affinity labeling and trypsin digestion. *Eur J Biochem.*; **251**: 682–90.

Murakami K, Tanabe K, Takada S. (1990) Structure of plasmodium yoelii gene-encoded protein homologous to the Ca^{2+}-ATPase of rabbit skeletal muscle sarcoplasmic reticulum. *J Cell Sci.*; **97**: 487–95.

Myung J, Jencks WP. (1994) Lumenal and cytoplasmic binding sites for calcium on the calcium ATPase of sarcoplasmic reticulum are different and independent. *Biochemistry.*; **33**: 8775–85.

Myung J, Jencks WP. (1995) There is only one phosphoenzyme intermediate with bound calcium on the reaction pathway of the sarcoplasmic reticulum calcium ATPase. *Biochemistry.*; **34**: 3077–83.

Newton T, Black JP, Butler J, Lee AG, Chad J, East JM. (2003) Sarco/endoplasmic-reticulum calcium ATPase SERCA1 is maintained in the endoplasmic reticulum by a retrieval signal located between residues 1 and 211. *Biochem J.*; **371**: 775–82.

Ogawa H, Stokes DL, Sasabe H, Toyoshima C. (1998) Structure of the Ca^{2+}-pump of sarcoplasmic reticulum: a view along the lipid bilayer at 9 Å resolution. *Biophys J.*; **75**: 41–52.

Ogawa H, Toyoshima C. (2002) Homology modelling of the cation binding sites of Na^{+},K^{+}-ATPase. *Proc Natl Acad Sci USA.*; **99**: 15977–82.

Ogurusu T, Wakabayashi S, Shigekawa M. (1991) Functional characterization of lanthanide binding sites in the sarcoplasmic

reticulum Ca^{2+}-ATPase: do lanthanide ions bind to the calcium transport site? *Biochemistry.*; **30**: 9966–73.

Ohnoki S, Martonosi A. (1980) Structural differences bvetween Ca^{2+} transport ATPases isolated from sarcoplasmic reticulum of rabbit, chicken and lobster muscle. *Comp Biochem Physiol B.*; **65**: 181–9.

Palmero I, Sastre L. (1989) Complementary DNA cloning of a protein highly homologous to mammalian sarcoplasmic reticulum Ca-ATPase from the crustacean Artemia. *J Mol Biol.*; **210**: 737–48.

Papp S, Pikula S, Martonosi A. (1987) Fluorescence energy transfer as an indicator of Ca^{2+}-ATPase interactions in sarcoplasmic reticulum. *Biophys J.*; **51**: 205–20.

Pascolini D, Blasie JK. (1988) Moderate resolution profile structure of the sarcoplasmic reticulum membrane under low temperature conditions for the transient trapping of $E_1 \cdot P$. *Biophys J.*; **54**: 669–78.

Pascolini D, Herbette LG, Skita V, Asturias F, Scarpa A, Blasie JK. (1988). Changes in the sarcoplasmic reticulum membrane profile indeced by enzyme phosphorylation to $E_1 \cdot P$ at 16 Å resolution *via* time-resolved X-ray diffraction. *Biophys J.*; **54**: 679–88.

Peachey LD, Franzini-Armstrong C. (1983) Structure and function of membrane systems of skeletal muscle cells. In *Handbook of physiology, Section 10, Skeletal Muscle*. Peachey LD, Adrian RH, eds, pp 23–71. Bethesda, American Physiological Society.

Peracchia C, Dux L, Martonosi A. (1984) Crystallization of intramembrane particles in rabbit sarcoplasmic reticulum vesicles by vanadate. *J Muscle Res Cell Motil.*; **5**: 431–42.

Pick U. (1981) Interaction of fluorescein isothiocyanate with nucleotide binding sites of the Ca^{2+} ATPase from sarcoplasmic reticulum. *Eur J Biochem.*; **121**: 187–195.

Pikula S, Mullner N, Dux L, Martonosi A. (1988) Stabilization and crystallization of Ca^{2+}-ATPase in detergent-solubilized sarcoplasmic reticulum. *J Biol Chem.*; **263**: 5277–86.

Pikula S, Wrzosek A, Famulski KS. (1991) Long-term stabilization and crystallization of (Ca^{2+} + Mg^{2+})-ATPase of detergent solubilized erythrocyte plasma membrane. *Biochim Biophys Acta.*; **1061**: 206–14.

Rice WJ, Young HS, Martin DW, Sacks JR, Stokes DL. (2001) Structure of Na^+,K^+-ATPase at 11 Å resolutionn: comparison with Ca^{2+}-ATPase in E1 and E2 states. *Biophys J.*; **80**: 2187–97.

Sagara Y, Wade JB, Inesi G. (1992) A conformational mechanism for formation of a dead-end complex by the sarcoplasmic reticulum Ca^{2+}-ATPase with thapsigargin. *J Biol Chem.*; **267**: 1286–92.

Serpersu EH, Kirch U, Schoner W. (1982) Demonstration of a stable occluded form of Ca^{2+} by the use of the chromium complex of ATP in the Ca^{2+}-ATPase of sarcoplasmic reticulum. *Eur J Biochem.*; **122**: 347–54.

Shi D, Hsiung H-H, Pace RC, Stokes DL. (1995) Preparation and analysis of large, flat crystals of Ca^{2+}-ATPase for electron crystallography. *Biophys J.*; **68**: 1152–62.

Shi D, Lewis MR, Young HS, Stokes DL. (1998) Three dimensional crystals of Ca^{2+} ATPase from sarcoplasmic reticulum: merging electron diffraction tilt series and imaging the (h, k, o) projection. *J Mol Biol.*; **284**: 1547–64.

Shull GE, Schwartz A, Lingrell JB. (1985) Amino-acid sequence of the catalytic subunit of the (Na^+ + K^+)-ATPase deduced from a complementary DNA. *Nature.*; **316**: 691–5.

Soulie S, Neumann JM, Berthomien C, Moller JV, le Maire M, Forge V. (1999) NMR conformational study of the sixth transmembrane segment of sarcoplasmic reticulum Ca^{2+}-ATPase. *Biochemistry.*; **38**: 5813–21.

Stokes DL, Green NM. (1990a) Structure of CaATPase: electron microscopy of frozen-hydrated crystals at 6 Å resolution in projection. *J Mol Biol.*; **213**: 529–38.

Stokes DL, Green NM. (1990b) Three-dimensional crystals of CaATPase from

sarcoplasmic reticulum. Symmetry and molecular packing. *Biophys J.*; **57**: 1–14.

Stokes DL, Green NM. (2000) Modeling a dehalogenase fold into the 8 Å density map for Ca^{2+}-ATPase defines a new domain structure. *Biophys J.*; **78**: 1765–76.

Stokes DL, Lacapere J-J. (1994) Conformation of Ca^{2+}-ATPase in two crystal forms. Effects of Ca^{2+}, thapsigargin, adenosine-5′(β,γ methylene) triphosphate and chromium (III)-ATP on crystallization. *J Biol Chem.*; **269**: 11606–13.

Sweadner KJ, Donnet C. (2001) Structural similarities of NaK-ATPase and SERCA, the Ca^{2+}-ATPase of the sarcoplasmic reticulum. *Biochem J.*; **356**: 685–704.

Taylor KA, Dux L, Martonosi A. (1984) Structure of the vanadate-induced crystals of sarcoplasmic reticulum Ca^{2+}-ATPase. *J Mol Biol.*; **174**: 193–204.

Taylor KA, Dux L, Martonosi A. (1986a) Three-dimensional reconstruction of negatively stained crystals of the Ca^{2+}-ATPase from muscle sarcoplasmic reticulum. *J Mol Biol.*; **187**: 417–27.

Taylor KA,. Dux L, Varga S, Ting-Beall HP, Martonosi A. (1988a) Analysis of two-dimensional crystals of Ca^{2+}-ATPase in sarcoplasmic reticulum. *Methods Enzymol.*; **157**: 71–289.

Taylor KA, Ho M-H, Martonosi A. (1986b) Image analysis of Ca^{2+}-ATPase from sarcoplasmic reticulum. *Ann NY Acad Sci.*; **483**: 31–43.

Taylor KA, Mullner N, Pikula S, Dux L, Peracchia C, Varga S, Martonosi A. (1988b) Electron microscope observations on Ca^{2+}-ATPase microcrystals in detergent-solubilized sarcoplasmic reticulum. *J Biol Chem.*; **263**: 5287–94.

Taylor KA, Varga S. (1994) Similarity of 3-dimensional microcrystals of detergent-solubilized (Na^+,K^+)-ATPase from pig kidney and Ca^{2+}-ATPase from skeletal muscle sarcoplasmic reticulum. *J Biol Chem.*; **269**: 10107–11.

Tillack TW, Boland R, Martonosi A. (1974) The ultrastructure of developing sarcoplasmic reticulum. *J Biol Chem.*; **249**: 624–33.

Ting-Beall HP, Burgess FM, Dux L, Martonosi A. (1987) Electron microscopic analysis of two dimensional crystals of the Ca^{2+}-transport ATPase - a freeze facture study. *J Muscle Res Cell Motil.*; **8**: 252–9.

Tong SW. (1977) The acetylated NH_2 terminus of Ca-ATPase from rabbit skeletal muscle sarcoplasmic reticulum: A common NH_2 terminal acetylated methionyl sequence. *Biochem Biophys Res Commun.*; **74**: 1242–8.

Tong SW. (1980) Studies on the structure of the calcium-dependent adenosine triphosphatase from rabbit skeletal muscle sarcoplasmic reticulum. *Arch Biochem Biophys.*; **203**: 780–91.

Toyoshima C, Nomura H, Sugita Y. (2003) Crystal structures of Ca^{2+}-ATPase in various physiological states. *Ann N Y Acad Sci.*; **986:** 1–8.

Toyoshima C, Nakasake M, Nomura H, Ogawa H. (2000) Crystal structure of the calcium pump of sarcoplasmic reticulum at 2.6 Ĺ resolution. *Nature.*; **405**: 647–55.

Toyoshima C, Nomura H. (2002) Structural changes in the calcium pump accompanying the dissociation of calcium. *Nature.*; **418**: 605–11.

Toyoshima C, Sasabe H, Stokes DL. (1993) Three-dimensional cryo-electron microscopy of the calcium ion pump in the sarcoplasmic reticulum membrane. *Nature.*; **362**: 469–71.

Vanderkooi JM, Ierokomas A, Nakamura H, Martonosi. (1977) Fluorescence energy transfer between Ca^{2+} transport ATPase molecules in artificial membranes. *Biochemistry.*; **16**: 1262–7.

Varga S. (1993) 3-dimensional (Type I) microcrystals of detergent-solubilized (Na^+,K^+)-ATPase enzyme from pig kidney. *Acta Physiol Hung.*, **81**: 409–24.

Varga S. (1994) Three-dimensional (Type I) microcrystals of detergent-solubilized membrane-bound gastric (H^+,K^+)-ATPase enzyme

from hog and rabbit stomachs. *Acta Physiol Hung.*; **82**: 365–76.

Varga S, Csermely P, Martonosi A. (1985) The binding of vanadium (V) oligoanions to sarcoplasmic reticulum. *Eur J Biochem.*; **148**: 119–26.

Varga S, Martonosi A. (1992) Giant sarcoplasmic reticulum vesicles: a study of membrane morphogenesis. *J Muscle Res Cell Motil.*; **13**: 497–510.

Varga S, Szabolcs M. (1994) Further characterization of the 3-dimensional crystals of detergent-solubilized (Na^+,K^+)-ATPase from pig kidney. *Acta Physiol Hung.*; 82: 139–52.

Varga S, Taylor KA, Martonosi A. (1991) Effects of solutes on the formation of crystalline sheets of the Ca^{2+}-ATPase in detergent-solubilized sarcoplasmic reticulum. *Biochim Biophys Acta.*; **1070**: 374–86.

Vegh M, Molnar E, Martonosi A. (1990) Vanadate catalysed, conformationnally specific photochemical cleavage of the Ca^{2+}-ATPase of sarcoplasmic reticulum. *Biochim Biophys Acta.*; **1023**: 168–183.

Verboomen H, Mertens L, Eggermont J, Wuytack F, Van Den Bosch L. (1995) Modulation of SERCA2 activity: regulated splicing and interaction with phospholamban. *Biosci Rep.*; **15**: 307–15.

Vilsen B. (1995) Structure-function relationships in the Ca^{2+}-ATPase of sarcoplasmic reticulum, studied by use of the substrate analogue CrATP and site directed mutagenesis comparison with Na^+,K^+-ATPase. *Acta Physiol Scand.*; **154**:Suppl 624, 1–146.

Vilsen B, Andersen JP. (1992) Interdependence of Ca^{2+} occlusion sites in the unphosphorylated sarcoplasmic reticulum Ca^{2+}-ATPase complex with CrATP. *J Biol Chem.*; **267**: 3539–50.

Weber A. (1959) On the role of calcium in the activity of adenosine-5'-triphosphate hydrolysis by actomyosin. *J Biol Chem.*; **234**: 2764–9.

Weber A, Herz R, Reiss I. (1964) The regulation of myofibrillar activity by calcium. *Proc Roy Soc London Series B.*; **160**: 489–501.

Wu K-D, Lee W-F, Wey J, Bungard D, Lytton J. (1995) Localization and quantification of endoplasmic reticulum Ca^{2+}-ATPase isoform transcripts. *Am J Physiol.*; **269**: C775–C784.

Wuytack F, Dode L, Baba-Aissa F, Raeymaekers L. (1995) The SERCA3 type organellar Ca^{2+} pumps. *Biosci Rep.*; 15: 299–305.

Xu C, Rice WJ, He W, Stokes DL (2002) A structural model for the catalytic cycle of Ca^{2+}-ATPase. *J Mol Biol.*; **316**: 201–11.

Yamamoto H, Imamura Y, Tagaya M, Fukui T, Kawakita M. (1989) Ca^{2+}-dependent conformational change of the ATP binding site of Ca^{2+} transporting ATPase of sarcoplasmic reticulum as revealed by an alteration of the target-site specificity of adenosinne triphosphopyridoxal. *J Biochem.*; **106**: 1121–5.

Yonekura K, Stokes DL, Sasabe H, Toyoshima C. (1997) The ATP-binding site of Ca^{2+}-ATPase revealed by electron image analysis. *Biophys J.*; **72**: 997–1005.

Young HS, Jones LR, Stokes DL. (2001) Locating phospholamban in co-crystals with Ca^{2+}-ATPase by cryoelectron microscopy. Biophys J.; **81**: 884–94.

Yu M, Zhang L, Rishi AK, Khadeer M, Inesi G, Hussain A. (1998) Specific substitutions at amino acid 256 of the sarcoplasmic/endoplasmic reticulum Ca^{2+} transport ATPase mediate resistance to thapsigargin in thapsigargin-resistant hamster cells. *J Biol Chem.*; **273**: 3542–6.

Yuul B, Juul B, Turc H, Durand ML, Gomez de Gracia A, Denoroy L, Moller JV, Champeil P, le Maire M. (1995) Do transmembrane segments in proteolyzed sarcoplasmic reticulum Ca^{2+}-ATPase retain their functional Ca^{2+} binding properties after removal of cytoplasmic fragments by proteinase K. *J Biol Chem.*; **270**: 20123–34.

Zhang Z, Lewis D, Sumbilla C, Inesi G and Toyoshima C. (2001) The role of the M6-M7 loop (L67) in stabilization of the phosphorylation and Ca^{2+} binding domains of the sarcoplasmic reticulum Ca^{2+}-ATPase (SERCA). *J Biol Chem.*; **276**: 15232–9.

Zhang P, Toyoshima C, Yonekura K, Green NM, Stokes DL. (1998) Structure of the calcium pump from sarcoplasmic reticulum at 8 Å resolution. *Nature.*; **392**: 835–9.